ARMY RESEARCH LABORATORY

Turbulence Models and the Synthesis of Random Fields for Acoustic Wave Propagation Calculations

by D. Keith Wilson

ARL-TR-1677 July 1998

The findings in this report are not to be construed as an official Department of the Army position unless so designated by other authorized documents.

Citation of manufacturer's or trade names does not constitute an official endorsement or approval of the use thereof.

Destroy this report when it is no longer needed. Do not return it to the originator.

Army Research Laboratory
Adelphi, MD 20783-1197

ARL-TR-1677 **July 1998**

Turbulence Models and the Synthesis of Random Fields for Acoustic Wave Propagation Calculations

D. Keith Wilson
Information Science and Technology Directorate

Abstract

A comprehensive set of equations is derived for correlations and spectra of atmospheric turbulence, useful for wave propagation calculations and other applications. Three basic turbulence models are considered: the Gaussian, von Kármán, and Kolmogorov models. Two extended forms of the von Kármán model are also described: the Mann model for a shear-driven atmospheric surface layer, and the Hunt/Graham/Wilson model for a convective boundary layer. A new method for synthesizing random fields from an inhomogeneous spectral model, called the generalized random-phase method, is described and applied to the various turbulence models.

Contents

Figures

1. Introduction

Atmospheric turbulence interferes with the coherent propagation of acoustic and electromagnetic waves. As a result, turbulence becomes important in many problems involving detection, identification, and location of targets. Statistical models of turbulence, which are useful for incorporation into wave propagation and scattering calculations, are the subject of this report.

The report is intended mainly as a reference document: it brings together a comprehensive collection of results from turbulence spectral modeling relevant to wave propagation calculations. Many of the results have not been previously published, or are scattered among diverse publications. A secondary purpose of the report is to provide a unified and systematic derivation of several statistical turbulence models, as well as methods for synthesizing random fields from these models. The report should be useful to readers having only modest familiarity with turbulence theory (for example, readers whose specialty is wave propagation) by providing a condensed tutorial on turbulence spectral theory and modeling.

The motivation for assembling these results is the strong interest that has developed during the past several years, particularly in acoustics, in incorporating realistic turbulence models into scattering calculations. This interest has been driven by the developing capability of computers and software to accurately calculate atmospheric turbulence effects on sound fields. An important example application is the scattering of sound into an acoustic shadow zone.* Shadow zones are created by topographic features (such as hills) or by refraction. Recent research (Gilbert et al., 1990, Juvé et al., 1994, Gilbert et al., 1996) has demonstrated that most sound energy reaching a receiver in an acoustic shadow is scattered there by turbulence, and that the simple, Gaussian models favored in the past do not describe the scattered signal levels well. Accurate calculation of sound fields therefore requires realistic turbulence models.

By *turbulence model*, I mean a set of equations or an algorithm that mimics statistical or dynamical properties of turbulence. Because of the complex nature of turbulence, there is no perfect model. Therefore, the usual approach to studying turbulence is to try to develop approximate models for

*In analogy to an optical shadow, an *acoustic shadow zone* is defined as a region not directly penetrated by rays of sound.

the particular properties of interest. This report is limited to second-order, two-point statistics of turbulence: correlation functions, spectra, and structure functions. These are the statistics normally needed to calculate *mean* sound levels in acoustic shadow zones, and to calculate signal coherence at an array of sensors. Some applications, such as the modeling of sound level *fluctuations* in shadow zones, require turbulence statistics higher than second order; however, such higher order models are beyond the scope of this report.

In this report I develop second-order statistical model equations by using a prescribed equation for the *specific energy spectrum*[*] as a starting point. I chose this approach because it leads to well-determined and straightforward modeling procedures. Alternative procedures for developing turbulence models are however possible: for example, one can define models by starting from correlation functions. A disadvantage with this alternative is that it can lead to confusion when vector fields are involved. Furthermore, I show in this report how the energy spectral approach can save some work in deriving model results needed for scattering, particularly for an important quantity called the two-dimensional (2D) correlation function.

Regardless of how the turbulence model is defined, the fundamental difficulty in modeling second-order turbulence statistics lies in realistic modeling of the energy subrange. This part of the turbulence spectrum, consisting of the largest eddies in the flow, is directly affected by the instability driving the turbulence. Since instability mechanisms that drive turbulence (primarily wind shear and density gradients) are inherently directional forces, statistics of the energy subrange eddies are anisotropic (dependent on direction). Statistics of the energy subrange are also highly flow dependent. The anisotropy and nonuniversality hamper development of universal parameterizations for energy subrange statistics.

Eventually the energy subrange eddies break down into the smaller eddies of the *inertial subrange*, and the "memory" of the instability mechanism that created the turbulence is lost. As a result, the inertial subrange is isotropic and amenable to universal parameterizations. Using Kolmogorov's (1941) scaling hypotheses, it is not difficult to develop realistic turbulence models for the inertial subrange.

The inertial subrange eddies continue to break down into smaller ones, until they are so small that molecular dissipation processes convert the turbulent energy to heat. This transition occurs at eddy sizes of 1 to 10 mm in the atmosphere. These small, dissipating eddies make up the *dissipation*

[*] *Specific* here means per unit mass. For example, the specific kinetic energy of a moving parcel of fluid is $v^2/2$, where v is the speed of the parcel.

subrange. Modeling of the dissipation subrange is not considered in this report, because sound waves that are useful for long-range detection have characteristic wavelengths that are much larger than the dissipation subrange eddies and therefore play an insignificant role in scattering.

I consider several turbulence models, which capture the turbulence features discussed above with varying degrees of realism:

1. Isotropic Gaussian model. This is the simplest reasonable model from an analytical standpoint. All the desired results are easily obtained in closed form. The disadvantage of the Gaussian model is that it is unrealistic for the inertial subrange. The energy in high-Reynolds-number turbulence, such as the atmosphere, is distributed over a broad range of spatial scales, although in the Gaussian model all the energy is concentrated at a single length scale. The Gaussian model is discussed in this report mainly for reference purposes.*

2. Von Kármán model. This model has a realistic inertial subrange. The energy subrange, although mathematically well behaved, is somewhat unrealistic since it is isotropic. All second-order statistics of interest can be obtained analytically, although the mathematical manipulations become rather complicated.

3. Kolmogorov model. This model is intended only for the inertial subrange, for which it is both realistic and simple. One drawback, in comparison to the von Kármán model, is that many of the equations diverge in the energy subrange. Therefore some care must be taken in applying the Kolmogorov model. All results for the Kolmogorov model actually can be obtained from calculations of high-wavenumber approximations to the von Kármán model, as well as by other methods. The Kolmogorov model can be expressed entirely in terms of a single parameter, called the structure-function parameter. This feature has proven convenient in previous experimental and theoretical studies of scattering.

4. HGW (Hunt/Graham/Wilson) model. Hunt and Graham (1978, 1984) developed a method to determine the modification of free-space spectra due to blocking (damping of the vertical velocity) at a plane boundary such as the ground. The boundary was modeled as a flat, free-slip surface. In previous work (Wilson, 1997c), I applied the Hunt and Graham method (with the von Kármán model used for

*One advantage of the Gaussian model is that it is particularly easy to formulate an anisotropic version. As a result, it may work reasonably well for the energy subrange in some situations (Wilson & Thomson, 1994). In this report, however, I consider only the isotropic Gaussian model.

the free-space spectra) to the atmospheric, convective boundary layer (CBL). The HGW model is an example of a vertically inhomogeneous (height-dependent) model. A disadvantage of the HGW model is that many statistics of interest must be obtained by numerical integration.

5. Mann model. Mann (1994) developed a theory for the distortion of turbulence by a constant wind shear. The theory agrees quite well with spectra recorded near the ground on a windy day. Like the HGW model, the Mann model requires numerical integrations to compute most statistics needed for wave propagation studies.

Models 1 to 3 actually take on slightly different forms, depending on whether the turbulent field of interest is scalar or vector. Models 4 and 5 apply only to turbulent velocity fluctuations (a vector field).

For each turbulence model, several statistical functions of interest must be derived:

1. 1D correlations and spectra. Although these are actually of little intrinsic interest in wave propagation calculations, it is typical of field measurements that the only turbulence data available are time series recorded by fixed sensors on a vertical tower. The time series can be converted to 1D spatial series via Taylor's hypothesis ($\Delta x = V\Delta t$, where V is the wind speed, and Δx and Δt are the increments in space and time, respectively). From calculations of spectra and/or correlations from the 1D spatial series, the parameters for the turbulence model can be determined. Hence 1D spectra and correlations are indirectly valuable.

2. 2D correlation function. This function is needed for computing the mutual coherence function, which describes the coherence between the signals at spatially separated microphones. The coherence between the microphones is needed for calculating the effects of turbulence on sensor arrays (Wilson, 1997a).

3. 2D spectrum. Numerical calculations of acoustic propagation through turbulence are frequently performed in a 2D plane in order to alleviate the demand on computational resources. The plane used in the calculation is normally a vertical one, with the nominal direction of propagation being the horizontal coordinate. A 2D turbulence spectrum in the plane of calculation is needed to "synthesize" a random field having the same second-order statistics as the turbulence model.

4. 3D spectrum. Most treatments of volume scattering require the 3D spectrum for calculations of the scattered field. For homogeneous

turbulence, the 3D spectrum can be used to synthesize a 3D random field.

5. 2D cross spectrum. This is the generalization of the 3D spectrum to vertically inhomogeneous turbulence. The 2D cross spectrum is a spectrum with regard to the horizontal variables, and a correlation function in the vertical direction. Inhomogeneous, 3D random fields can be synthesized from the 2D cross spectrum by a method discussed in section 3.

This report is structured as follows. Following a brief exposition of some of the fundamental concepts and equations involved in modeling turbulence spectra (sect. 2), I discuss a method for synthesizing a random turbulent field from a prescribed homogeneous or inhomogeneous spectrum (sect. 3). The next five sections each discuss one of the five turbulence models mentioned above. Section 9 gives some examples of synthesized random fields, generated by the various turbulence models.

2. General Principles

This section provides some general background on modeling turbulence correlations and spectra.

2.1 Correlation and 3D Spectral Functions

Let us define the correlation function of a random, scalar field s as

$$R\left(x_1, x_1', x_2, x_2', x_3, x_3'\right) = \left\langle s\left(x_1, x_2, x_3\right) s\left(x_1', x_2', x_3'\right)\right\rangle, \tag{1}$$

where the angle brackets indicate ensemble averaging. If the field is *homogeneous*, by definition the correlation function depends only on the separations between the measurement points, $r_i = x_i' - x_i$. Then we can make the simplification

$$R\left(r_1, r_2, r_3\right) = R\left(x_1, x_1', x_2, x_2', x_3, x_3'\right). \tag{2}$$

If the field is also *isotropic* (i.e., its statistics are independent of coordinate rotations), then the correlation function of a scalar depends only on the radial distance r between the measurement points, where $r^2 = r_1^2 + r_2^2 + r_3^2$. For a homogeneous, isotropic scalar field, one can therefore define a normalized correlation function $h\left(r\right)$ such that

$$\sigma^2 h\left(r\right) = R\left(r_1, r_2, r_3\right). \tag{3}$$

The 3D spectral density function $\Phi\left(\kappa_1, \kappa_2, \kappa_3\right)$ (spectrum, for short) can be defined as the 3D Fourier transform of the correlation function:

$$\begin{aligned} \Phi\left(\kappa_1, \kappa_2, \kappa_3\right) \;=\; & \frac{1}{8\pi^3} \int_{-\infty}^{\infty}\int_{-\infty}^{\infty}\int_{-\infty}^{\infty} R\left(r_1, r_2, r_3\right) \\ & \times \exp\left[-i\left(\kappa_1 r_1 + \kappa_2 r_2 + \kappa_3 r_3\right)\right] dr_1\, dr_2\, dr_3, \end{aligned} \tag{4}$$

$$\begin{aligned} R\left(r_1, r_2, r_3\right) \;=\; & \int_{-\infty}^{\infty}\int_{-\infty}^{\infty}\int_{-\infty}^{\infty} \Phi\left(\kappa_1, \kappa_2, \kappa_3\right) \\ & \times \exp\left[i\left(\kappa_1 r_1 + \kappa_2 r_2 + \kappa_3 r_3\right)\right] d\kappa_1\, d\kappa_2\, d\kappa_3, \end{aligned} \tag{5}$$

where κ_i is the wavenumber in the direction of r_i.

Vector quantities, such as turbulent velocity fluctuations, are handled similarly to scalars. However, the situation becomes somewhat more complicated for vectors, since three directions are involved in a given spectrum

or correlation: the direction of the displacement and the orientations of the two velocity components. (Only the direction of the displacement is involved in the scalar case.) Let us define the correlation function of a homogeneous vector field as

$$R_{ij}\left(r_1, r_2, r_3\right) = \left\langle u_i\left(x_1, x_2, x_3\right) u_j\left(x_1', x_2', x_3'\right)\right\rangle, \tag{6}$$

where the subscripts *i* and *j* indicate the velocity component. Note that R_{ij} is a tensor quantity, having nine components. We can define the spectral density by taking Fourier transforms in a manner analogous to the scalar case.

Unlike scalar fields, vector fields (even if isotropic) do not have the property that the correlation functions depend only on r. However, it is true for an isotropic vector field that $R_{11}\left(r,0,0\right) = R_{22}\left(0,r,0\right) = R_{33}\left(0,0,r\right)$. Hence for vectors we define the correlation function $f\left(r\right)$ by the relationship

$$\sigma^2 f\left(r\right) = R_{11}\left(r,0,0\right), \text{ etc.} \tag{7}$$

In this case, $f\left(r\right)$ is referred to as the normalized *longitudinal* correlation function, so that it can be distinguished from correlations such as $R_{22}\left(r,0,0\right)$ and $R_{33}\left(0,r,0\right)$, where the velocity components and displacement are perpendicular to each other. Let us define a normalized *lateral* correlation function $g\left(r\right)$ such that

$$\sigma^2 g\left(r\right) = R_{22}\left(r,0,0\right), \text{ etc.} \tag{8}$$

A further complication when dealing with turbulent velocities, in comparison to scalar fields, is that the elements of the correlation or spectral tensor cannot be specified independently. Conservation of mass and nondivergence of the flow impose interrelationships between the tensor elements. In fact, the longitudinal and lateral correlations are related by the equation (Batchelor, 1953)

$$g\left(r\right) = f\left(r\right) + \frac{r}{2}\frac{df}{dr}. \tag{9}$$

The full correlation tensor, in terms of the longitudinal and lateral correlations, is (Batchelor, 1953)

$$R_{ij}\left(r_1, r_2, r_3\right) = \sigma^2\left[\frac{r_i r_j}{r^2} f\left(r\right) + \left(\delta_{ij} - \frac{r_i r_j}{r^2}\right) g\left(r\right)\right]. \tag{10}$$

2.2 Energy Spectra

A particularly convenient way to deal with some of the differences between the cases of scalar and vector random fields is to define turbulence models based on their *energy spectra*, rather than their correlation functions. The energy spectrum $E\left(\kappa\right)$ is defined such that its integral over the wavenumber

κ (where $\kappa^2 = \kappa_1^2 + \kappa_2^2 + \kappa_3^2$) equals one-half of the total variance of the field. For a scalar quantity s,

$$\int_0^\infty E_s(\kappa)\, d\kappa = \frac{\sigma^2}{2}. \tag{11}$$

Note from the Fourier transform relation, equation (5), with $r_1 = r_2 = r_3 = 0$,

$$\sigma^2 = \int_{-\infty}^{\infty}\int_{-\infty}^{\infty}\int_{-\infty}^{\infty} \Phi(\kappa_1, \kappa_2, \kappa_3)\; d\kappa_1\; d\kappa_2\; d\kappa_3.$$

Hence we can find the isotropic 3D spectrum $\Phi(\kappa)$ by multiplying $E_s(\kappa)$ by two, and then dividing by the "area" of a spherical shell in wavenumber space, $4\pi\kappa^2$:

$$\Phi(\kappa) = \frac{E_s(\kappa)}{2\pi\kappa^2}. \tag{12}$$

Substituting into equation (5), we see that we can compute the correlation function for a scalar from the energy spectrum using

$$\begin{aligned} R(r_1, r_2, r_3) \;=\; & \int_{-\infty}^{\infty}\int_{-\infty}^{\infty}\int_{-\infty}^{\infty} \frac{E_s(\kappa)}{2\pi\kappa^2} \\ & \times \exp\left[i\left(\kappa_1 r_1 + \kappa_2 r_2 + \kappa_3 r_3\right)\right]\; d\kappa_1\; d\kappa_2\; d\kappa_3. \end{aligned} \tag{13}$$

Because of isotropy, we can also set $r_1 = r$, $r_2 = 0$, and $r_3 = 0$, before the integration. Hence

$$h(r) = \frac{1}{\sigma^2}\int_{-\infty}^{\infty}\int_{-\infty}^{\infty}\int_{-\infty}^{\infty} \frac{E_s(\kappa)}{2\pi\kappa^2} \exp(i\kappa_1 r)\; d\kappa_1\; d\kappa_2\; d\kappa_3. \tag{14}$$

In the case of vectors, such as the turbulent velocities, the energy spectrum $E_v(\kappa)$ is defined such that

$$\int_0^\infty E_v(\kappa)\, d\kappa = \frac{3\sigma^2}{2}. \tag{15}$$

The reason for incorporating the factor 3 is that the total variance in the field equals $3\sigma^2$, if σ^2 is defined as the variance in just one of the three velocity components. For a nondivergent, mass-conserving flow, the 3D spectra are related to the energy spectrum according to (Batchelor, 1953)

$$\Phi_{ij}(\boldsymbol{\kappa}) = \frac{E_v(\kappa)}{4\pi\kappa^4}\left(\delta_{ij}\kappa^2 - \kappa_i\kappa_j\right). \tag{16}$$

From this equation it can be shown, analogously to the scalar case, that

$$\Phi_{11}(\boldsymbol{\kappa}) + \Phi_{22}(\boldsymbol{\kappa}) + \Phi_{33}(\boldsymbol{\kappa}) = \frac{E_v(\kappa)}{2\pi\kappa^2}.$$

The equation for the correlation function of a vector quantity, in terms of the energy spectrum, is slightly more complicated than the scalar result:

$$R_{ij}\left(r_1, r_2, r_3\right) = \int_{-\infty}^{\infty}\int_{-\infty}^{\infty}\int_{-\infty}^{\infty} \frac{E_v\left(\kappa\right)}{4\pi\kappa^4}\left(\delta_{ij}\kappa^2 - \kappa_i\kappa_j\right) \times \exp\left[i\left(\kappa_1 r_1 + \kappa_2 r_2 + \kappa_3 r_3\right)\right]\, d\kappa_1\, d\kappa_2\, d\kappa_3. \tag{17}$$

From equation (17), we have for vectors

$$f(r) = \frac{1}{\sigma^2}\int_{-\infty}^{\infty}\int_{-\infty}^{\infty}\int_{-\infty}^{\infty} \frac{E_v\left(\kappa\right)}{4\pi\kappa^4}\left(\kappa^2 - \kappa_1^2\right)\exp\left(i\kappa_1 r\right)\, d\kappa_1\, d\kappa_2\, d\kappa_3, \tag{18}$$

and

$$g(r) = \frac{1}{\sigma^2}\int_{-\infty}^{\infty}\int_{-\infty}^{\infty}\int_{-\infty}^{\infty} \frac{E_v\left(\kappa\right)}{4\pi\kappa^4}\left(\kappa^2 - \kappa_2^2\right)\exp\left(i\kappa_1 r\right)\, d\kappa_1\, d\kappa_2\, d\kappa_3. \tag{19}$$

2.3 2D Correlation Function

The *2D correlation function* is an important result for acoustic and electromagnetic wave propagation studies (Wilson, 1998). The 2D correlation function is defined as the 2D inverse Fourier transform of $\Phi\left(0, \kappa_2, \kappa_3\right)$,

$$b\left(\rho\right) = \int_{-\infty}^{\infty}\int_{-\infty}^{\infty} \Phi\left(0, \kappa_2, \kappa_3\right)\exp\left[i\left(\kappa_2 r_2 + \kappa_3 r_3\right)\right]\, d\kappa_2\, d\kappa_3, \tag{20}$$

where $\rho^2 = r_2^2 + r_3^2$. Equivalently, by Fourier transforming equation (5) with respect to r_1 and setting $\kappa_1 = 0$, one has

$$b\left(\rho\right) = \frac{1}{2\pi}\int_{-\infty}^{\infty} R\left(r_1, r_2, r_3\right)\, dr_1. \tag{21}$$

I should point out that most previous authors have called the 2D correlation function the *transverse correlation function*. Unfortunately, I have already used that term for the function $g\left(r\right)$. (Taxonomically speaking, the function $g\left(r\right)$ is a 3D correlation function, with the spatial separation transverse to the velocity components.) My reason for adopting the different terminology here (besides the name conflict) is that, since the 2D spectrum (discussed in sect. 2.4) is the 2D Fourier transform of $R\left(0, r_2, r_3\right)$, it only makes sense that the 2D inverse Fourier transform of $\Phi\left(0, \kappa_2, \kappa_3\right)$ should be called the 2D correlation function.

A second important point regarding equation (20) is that the integration could just as well have been over the plane $\left(\kappa_1, \kappa_2\right)$ (or $\left(\kappa_1, \kappa_3\right)$, for that matter) instead of $\left(\kappa_2, \kappa_3\right)$. Then the appropriate spectrum in the integral would be $\Phi\left(\kappa_1, \kappa_2, 0\right)$, and the spatial separation would be $\rho^2 = r_1^2 + r_2^2$. The two definitions are equivalent for isotropic fields.

The 2D correlation function can be found in terms of the energy spectrum by substitution of equation (12) into (20). The result is somewhat similar to equation (14) for the normalized correlation function, except that the integration over κ_1 is omitted, and r_1 is set to zero:

$$b(\rho) = \frac{1}{2\pi} \int_{-\infty}^{\infty} \int_{-\infty}^{\infty} \frac{E_s(\kappa_h)}{\kappa_h^2} \exp\left[i(\kappa_2 r_2 + \kappa_3 r_3)\right] \, d\kappa_2 \, d\kappa_3, \tag{22}$$

where $\kappa_h^2 = \kappa_2^2 + \kappa_3^2$. By rewriting this equation in polar coordinates over the plane (κ_2, κ_3), and then using the integral definition of the Bessel function (eq (9.1.21) in Abramowitz and Stegun, 1965), we can reduce the double integral to a single one:

$$b(\rho) = \int_0^{\infty} \frac{E_s(\kappa_h)}{\kappa_h} J_0(\kappa_h \rho) \, d\kappa_h. \tag{23}$$

The 2D correlation function for fluctuations in the velocity components *perpendicular* to the displacement can be found by substitution of $\Phi_{11}(\kappa)$, as given by equation (16), into the definition of the 2D correlation function, equation (20):

$$b_{\parallel}(\rho) = \frac{1}{4\pi} \int_{-\infty}^{\infty} \int_{-\infty}^{\infty} \frac{E_v(\kappa_h)}{\kappa_h^2} \exp\left[i(\kappa_2 r_2 + \kappa_3 r_3)\right] \, d\kappa_2 \, d\kappa_3 \tag{24}$$

$$= \frac{1}{2} \int_0^{\infty} \frac{E_v(\kappa_h)}{\kappa_h} J_0(\kappa_h \rho) \, d\kappa_h. \tag{25}$$

Note the similarity between equations (25) and (23) — the only differences are the factor of $1/2$ appearing in (25), and $E_v(\kappa_h)$ replacing $E_s(\kappa_h)$.

The 2D correlation function for velocity fluctuations in the plane of the displacement is found by substitution of either $\Phi_{22}(\kappa)$ or $\Phi_{33}(\kappa)$ into equation (20):

$$b_{\perp}(\rho) = \frac{1}{4\pi} \int_{-\infty}^{\infty} \int_{-\infty}^{\infty} \frac{E_v(\kappa_h)\,\kappa_2^2}{\kappa_h^4} \exp\left[i(\kappa_2 r_2 + \kappa_3 r_3)\right] \, d\kappa_2 \, d\kappa_3. \tag{26}$$

In the above, the roles of κ_2 and κ_3 can be switched without a change in the result. In any case, the function $b_{\perp}(\rho)$ appears to be of no importance in acoustic wave propagation calculations. The reason is that it is primarily the velocity components parallel to acoustic wavefronts that affect propagation. Hence $b_{\perp}(\rho)$ is discussed no further in this report.

2.4 1D and 2D Spectral Functions

As mentioned in the introduction, besides the 3D spectra, sometimes 1D and 2D spectra are needed for wave propagation studies. The 1D spectrum

is simply a 1D Fourier transform of the correlation function, with the displacements in the two untransformed directions set to zero. For a scalar,

$$\begin{aligned}\Theta(\kappa) &= \frac{1}{2\pi}\int_{-\infty}^{\infty} R(r,0,0)\exp(-i\kappa r)\ dr \\ &= \frac{\sigma^2}{2\pi}\int_{-\infty}^{\infty} h(r)\exp(-i\kappa r)\ dr. \end{aligned} \tag{27}$$

I indicate the normalized 1D spectrum for a scalar, $\Theta(\kappa)/\sigma^2$, with the notation $\hat{h}(\kappa)$.

Of course, in the case of vectors, the relative orientations between the velocity components and the displacements must be considered. In general, we have

$$\Theta_{ij}(\kappa_1) = \frac{1}{2\pi}\int_{-\infty}^{\infty} R_{ij}(r_1,0,0)\exp(-i\kappa_1 r_1)\ dr_1, \tag{28}$$

and likewise for the r_1 and r_2 directions. There are two cases of particular interest: one where the transformation is parallel to the velocity components,

$$\hat{f}(\kappa) = \frac{1}{2\pi}\int_{-\infty}^{\infty} f(r)\exp(-i\kappa r)\ dr = \Theta_{11}(\kappa_1)/\sigma^2, \text{ etc,} \tag{29}$$

and the other where it is perpendicular,

$$\hat{g}(\kappa) = \frac{\sigma^2}{2\pi}\int_{-\infty}^{\infty} g(r)\exp(-i\kappa r)\ dr = \Theta_{22}(\kappa_1)/\sigma^2, \text{ etc.} \tag{30}$$

Incidentally, equations (9), (10), and (16) can be used to show that the longitudinal spectrum is related to the energy spectrum according to

$$E_v(\kappa) = \sigma^2\kappa^3\frac{d}{d\kappa}\left[\frac{1}{\kappa}\frac{d\hat{f}(\kappa)}{d\kappa}\right]. \tag{31}$$

A generalization of the 1D spectrum that is sometimes useful in wave propagation studies is the 1D cross spectrum. Its definition is the same as that of the usual 1D spectrum, except that the arguments r_2 and r_3 in the correlation function are nonzero:

$$\Theta_{ij}(\kappa_1; r_2, r_3) = \frac{1}{2\pi}\int_{-\infty}^{\infty} R_{ij}(r_1,r_2,r_3)\exp(-i\kappa_1 r_1)\ dr_1. \tag{32}$$

The 2D spectrum is defined as the 2D Fourier transform of the correlation function. For a scalar,

$$\phi(\kappa_1,\kappa_2) = \frac{1}{4\pi^2}\int_{-\infty}^{\infty}\int_{-\infty}^{\infty} R(r_1,r_2,0)\exp[-i(\kappa_1 r_1+\kappa_2 r_2)]\ dr_1\ dr_2. \tag{33}$$

Assuming horizontal isotropy, and using the integral form of the Bessel function (e.g., eq (9.1.21) in Abramowitz and Stegun, 1965), one finds

$$\phi(\kappa_h) = \frac{\sigma^2}{2\pi} \int_0^\infty h(r)\, J_0(\kappa_h r)\, r\, dr, \tag{34}$$

in which $\kappa_h^2 = \kappa_1^2 + \kappa_2^2$. Alternatively, from the definitions of the Fourier transform and energy spectrum, it can be shown that

$$\begin{aligned} \phi(\kappa_1, \kappa_2) &= \int_{-\infty}^{\infty} \Phi(\kappa_1, \kappa_2, \kappa_3)\, d\kappa_3 \\ &= \int_0^\infty \frac{E_s(\kappa)}{\pi\kappa^2}\, d\kappa_3. \end{aligned} \tag{35}$$

The definition of the 2D spectrum for vectors is of course the same as equation (33), except that ϕ_{ij} and R_{ij} appear in place of ϕ and R. However, equations (34) and (35) do *not* hold. From equations (9), (10), and (16), it can be shown that

$$\begin{aligned} \phi_{11}(\kappa_1, \kappa_2) &= \frac{\sigma^2}{4\pi^2} \int_{-\infty}^{\infty}\int_{-\infty}^{\infty} \left\{ f(r) + \frac{r}{2}\left(1 + \frac{r_1^2}{r^2}\right)\frac{df}{dr} \right\} e^{-i(\kappa_1 r_1 + \kappa_2 r_2)}\, dr_1\, dr_2 \\ &= \int_0^\infty \frac{E_v(\kappa)}{2\pi\kappa^4}\left(\kappa^2 - \kappa_1^2\right) d\kappa_3, \quad \text{and} \end{aligned} \tag{36}$$

$$\begin{aligned} \phi_{33}(\kappa_1, \kappa_2) &= \frac{\sigma^2}{4\pi^2} \int_{-\infty}^{\infty}\int_{-\infty}^{\infty} g(r)\, e^{-i(\kappa_1 r_1 + \kappa_2 r_2)}\, dr_1\, dr_2 \\ &= \int_0^\infty \frac{E_v(\kappa)}{2\pi\kappa^4}\left(\kappa^2 - \kappa_3^2\right) d\kappa_3. \end{aligned} \tag{37}$$

In horizontally isotropic turbulence, the equations for $\phi_{22}(\kappa_1, \kappa_2)$ are the same as those for $\phi_{11}(\kappa_1, \kappa_2)$, except that the subscripts 1 and 2 are interchanged. Hence,

$$\phi_{22}(\kappa_1, \kappa_2) = \phi_{11}(\kappa_2, \kappa_1).$$

One of the turbulence models considered in this report (the HGW model, sect. 7) is vertically inhomogeneous. By definition, this means that equation (2) is invalid. The most simplified form of the correlation function is

$$R(r_1, r_2, z, z') = R(x_1, x_1', x_2, x_2', z, z'), \tag{38}$$

in which $z = x_3$ has been used for the vertical coordinate. Obviously, because of the inhomogeneity, we can no longer Fourier transform the correlation function with respect to the vertical coordinate. However, we can still Fourier transform with respect to the horizontal coordinates (x_1, x_2). The resulting spectrum is called the *2D cross spectrum*:

$$\phi\left(\kappa_1,\kappa_2;z,z'\right)=\frac{1}{4\pi^2}\int_{-\infty}^{\infty}\int_{-\infty}^{\infty}R\left(r_1,r_2,z,z'\right)\exp\left[-i\left(\kappa_1 r_1+\kappa_2 r_2\right)\right]\,dr_1\,dr_2. \tag{39}$$

The 2D cross spectrum for vectors is defined in the same way, except with subscript ij on the spectrum and correlation function. Note that when $z = z'$, the 2D cross spectrum reduces to the usual 2D spectrum. Also, when the turbulence is vertically homogeneous, the 2D cross spectrum depends only on the separation $r_3 = z' - z$.

2.5 Length Scales

It is important that we be able to consistently quantify length scales associated with given spectra. By *length scale*, I mean a value associated with the size of eddies from some part of the spectrum. One of the most useful length scales is the *integral length scale*, which characterizes the size of the most energetic eddies. For a scalar quantity, it is defined as

$$\mathcal{L}=\frac{1}{\sigma^2}\int_0^{\infty}R(r)\,dr=\int_0^{\infty}h(r)\,dr. \tag{40}$$

By setting $\kappa = 0$ in equation (27), one can derive the following simple relationship between the integral length scale and the 1D spectrum:

$$\mathcal{L}=\pi\widehat{h}\left(0\right). \tag{41}$$

The integral length scale and 2D correlation function are also simply related. From the Fourier transform relation between the correlation function and the spectrum, and from equation (12), we have

$$\frac{1}{2\pi}\int_{-\infty}^{\infty}R(r_1,0,0)\exp\left(-i\kappa_1 r_1\right)\,dr_1=\int_{-\infty}^{\infty}\int_{-\infty}^{\infty}\frac{E\left(\kappa\right)}{2\pi\kappa^2}\exp\left[\kappa_2 r_2+\kappa_3 r_3\right]\,d\kappa_2\,d\kappa_3.$$

Setting $r_2 = r_3 = 0$, and $\kappa_1 = 0$, and using the fact that $R(r_1, 0, 0)$ is an even function, we obtain

$$\frac{1}{\pi}\int_0^{\infty}R(r_1,0,0)\,dr_1=\frac{1}{2\pi}\int_{-\infty}^{\infty}\int_{-\infty}^{\infty}\frac{E\left(\kappa_h\right)}{\kappa_h^2}\,d\kappa_2\,d\kappa_3.$$

If this result is compared with equations (22) and (40), it is now evident that

$$\mathcal{L}=\frac{\pi}{\sigma^2}b\left(0\right). \tag{42}$$

In the vector case, the direction of the velocity components as well as the direction of the displacement must be considered. Two significant scales can be defined: one where the displacement is parallel to the velocity,

$$\mathcal{L}_{\parallel}=\int_0^{\infty}f(r)\,dr=\pi\widehat{f}\left(0\right), \tag{43}$$

and the other where it is perpendicular,

$$\mathcal{L}_{\perp} = \int_0^{\infty} g(r)\, dr = \pi \widehat{g}\,(0)\,. \tag{44}$$

For homogeneous, isotropic turbulence, it can be proven that (Batchelor, 1953)

$$\mathcal{L}_{\parallel} = 2\mathcal{L}_{\perp}. \tag{45}$$

Furthermore, using a derivation similar to the scalar case, one finds

$$\mathcal{L}_{\parallel} = \frac{\pi}{\sigma^2} b_{\parallel}\,(0)\,. \tag{46}$$

2.6 Structure Functions and Parameters

The structure function for an isotropic, homogeneous scalar field is defined as

$$D(r) = \left\langle [s\,(r) - s\,(0)]^2 \right\rangle. \tag{47}$$

For a vector, the structure function depends on the direction of the displacement:

$$D_{ij}(\mathbf{r}) = \left\langle [u_i\,(\mathbf{r}) - u_j\,(0)]^2 \right\rangle. \tag{48}$$

From the definitions, it is easily shown that

$$D\,(r) \;=\; 2\sigma^2 - 2R\,(r) = 2\sigma^2\,[1 - h\,(r)]\,, \quad \text{and} \tag{49}$$

$$D_{ij}(\mathbf{r}) \;=\; 2\sigma^2 - 2R_{ij}\,(\mathbf{r})\,. \tag{50}$$

For vectors, it is convenient to define

$$D_{\parallel}\,(r) \;=\; 2\sigma^2\,[1 - f\,(r)]\,, \quad \text{and} \tag{51}$$

$$D_{\perp}\,(r) \;=\; 2\sigma^2\,[1 - g\,(r)]\,. \tag{52}$$

Of particular interest is the structure function for small separations ($r \ll \mathcal{L}$). Based on Kolmogorov's (1941) scaling arguments, the structure functions should be proportional to $r^{2/3}$ in this limit. The ratio $D\,(r)\,/r^{2/3}$, for small r, is called the scalar *structure-function parameter* C_s^2. For vectors, a longitudinal displacement is used to define the structure-function parameter C_v^2. Hence,

$$C_s^2 \;=\; \lim_{r\to 0} \frac{2\sigma^2}{r^{2/3}}\,[1 - h\,(r)]\,, \quad \text{and} \tag{53}$$

$$C_v^2 \;=\; \lim_{r\to 0} \frac{2\sigma^2}{r^{2/3}}\,[1 - f\,(r)]\,. \tag{54}$$

Similar to the ordinary structure function is the 2D structure function, defined for scalars as

$$d(\rho) = 2[b(0) - b(\rho)], \tag{55}$$

and for vectors as

$$d_{\parallel}(\rho) = 2\left[b_{\parallel}(0) - b_{\parallel}(\rho)\right]. \tag{56}$$

The 2D structure function is needed for calculations of the mutual coherence function (see the introduction).

2.7 Energy Spectral Approach to Turbulence Modeling

In sections 2.1 to 2.6, I considered the interrelationships among various correlations, spectra, structure functions, and length scales that can be defined for random fields. Some care must be taken in devising a new statistical turbulence model so that none of the required relationships is violated. Actually, whether one is dealing with scalar or vector fields, only one correlation or spectral function can be uniquely specified; the others follow from the given relationships. The most obvious choices for the specified function are the following:

1. The energy spectrum $E(\kappa)$.
2. The scalar (or longitudinal) correlation $h(r)$ (or $f(r)$).
3. The scalar (or longitudinal) 1D spectral density $\widehat{h}(\kappa)$ (or $\hat{f}(\kappa)$).

The relationship between $E(\kappa)$ and $\hat{f}(\kappa)$ was given by equation (31). Of course, $f(r)$ and $\hat{f}(\kappa)$ are simply Fourier transform pairs. Equations for all the other correlations, spectra, etc, of interest, in terms of $E(\kappa)$ and/or $f(r)$ have already been discussed.

In the following sections of this report, I discuss several turbulence models derived from prescribed forms for the energy spectrum. The decision to use $E(\kappa)$, instead of either $f(r)$ or $\hat{f}(\kappa)$, is somewhat arbitrary. However, it does lead to somewhat simpler results for quantities such as the 2D correlation function, an advantage that I demonstrate shortly.

Suppose now that we use the same functional form for both the scalar and vector energy spectra, by setting*

$$E_v(\kappa) = 3E_s(\kappa). \tag{57}$$

*Of course, the scalar and vector fields can have different dimensions, in which case equation (57) is not satisfied dimensionally. But the equivalence I imply here is only a *functional* equivalence of the energy spectra. One can easily overcome any formal difficulties by nondimensionalizing the fields.

Let us consider what additional interrelationships between various scalar and vector results arise from making this assumption.

With regard to the correlation functions, by comparing equations (14), (18), and (19), we find

$$h(r) = \frac{1}{3}\left[f(r) + 2g(r)\right]. \tag{58}$$

The main utility of this equation is that it can reduce the work involved in determining the correlation functions. For example, suppose we perform the integrations specified by equation (18) to find $f(r)$. Next, equation (9) can be used to easily determine $g(r)$, and then equation (58) can be used to easily determine $h(r)$. This procedure is generally easier than solving equations (14), (18), and (19) individually.

By integrating equation (58), we can easily derive the following relationship for the integral length scales:

$$\mathcal{L} = \frac{1}{3}\left(\mathcal{L}_{\parallel} + 2\mathcal{L}_{\perp}\right) = \frac{2}{3}\mathcal{L}_{\parallel}. \tag{59}$$

Fourier transformation of equation (58) of course implies

$$\hat{h}(\kappa) = \frac{1}{3}\left[\hat{f}(\kappa) + 2\hat{g}(\kappa)\right]. \tag{60}$$

A generalized version of this equation can be derived for the 1D cross spectra. Using equation (10), one can show that $R_{11}(r_1, r_2, r_3) + R_{22}(r_1, r_2, r_3) + R_{33}(r_1, r_2, r_3) = \sigma^2\left[f(r) + 2g(r)\right]$. It then follows from equation (58) that

$$R(r_1, r_2, r_3) = \frac{1}{3}\left[R_{11}(r_1, r_2, r_3) + R_{22}(r_1, r_2, r_3) + R_{33}(r_1, r_2, r_3)\right]. \tag{61}$$

Fourier transformation of this equation with respect to r_1 yields

$$\Theta(\kappa_1, r_2, r_3) = \frac{1}{3}\left[\Theta_{11}(\kappa_1, r_2, r_3) + \Theta_{22}(\kappa_1, r_2, r_3) + \Theta_{33}(\kappa_1, r_2, r_3)\right]. \tag{62}$$

For the 2D correlation functions, substituting equation (57) into (24) and comparing to equation (22) yields the following result:

$$b_{\parallel}(\rho) = \frac{3}{2}b(\rho). \tag{63}$$

Hence, if we choose the same functional form for the energy spectrum for both the scalars and vectors, the resulting 2D correlation functions will be proportional to one another. This result can make wave propagation calculations much simpler.

If we apply a Fourier transform to equation (62) (with $r_3 = 0$), it follows for the 2D spectra that

$$\phi(\kappa_1, \kappa_2) = \frac{1}{3}\left[\phi_{11}(\kappa_1, \kappa_2) + \phi_{22}(\kappa_1, \kappa_2) + \phi_{33}(\kappa_1, \kappa_2)\right]. \tag{64}$$

Note also that $\phi_{11}(\kappa_2, \kappa_1) = \phi_{22}(\kappa_1, \kappa_2)$. Equation (64) also applies to the 2D cross spectra, after we make the notational change $\phi(\kappa_1, \kappa_2) \rightarrow \phi(\kappa_1, \kappa_2; z, z')$, etc.

For the 3D spectra, we have from equations (12) and (16)

$$\Phi_{ij}(\boldsymbol{\kappa}) = \frac{3}{2}\Phi(\kappa)\left(\delta_{ij}\kappa^2 - \kappa_i\kappa_j\right). \tag{65}$$

Equations (58) to (65) are helpful because they can reduce the amount of work required to derive various functions for a turbulence model. But it must be kept in mind that they are valid only when the energy spectra satisfy the functional equivalence relationship, equation (57). Other modeling procedures do not necessarily yield the same results.

3. Synthesis of Turbulence Using the Method of Random Phases

3.1 Motivation

During the past decade, acoustic propagation modeling has now advanced to the point where full-wave solutions can be computed for propagation through a medium having two- or three-dimensional spatial variability in the index-of-refraction field (e.g., Gilbert et al., 1990, Chevret et al., 1996). What is still needed, though, are realistic turbulence fields for input to these models.

Since a turbulence field cannot be directly measured to the fidelity needed for wave propagation calculations, some method for synthesizing turbulence is needed. Computer simulations of turbulence are available; in particular, the type of simulation called a large-eddy simulation (LES) has been successfully used to study atmospheric turbulence for the past two decades (Deardorff, 1970b, Moeng, 1984). LES is regarded as faithful to the atmosphere in most aspects. The difficulty with LES-generated data is the resolution, currently limited to about 30 m in the horizontal and 10 m in the vertical. Supposing that we need to resolve the turbulence field to better than 1/5 acoustic wavelength for reasonable calculations, the LES data would be useful for acoustic propagation modeling only at acoustic frequencies of about 6 Hz and lower. Therefore alternatives to LES are needed.

Gilbert et al. (1990) synthesized a planar turbulence field solely from its 2D spectrum, by multiplying the square root of the spectrum at each wavenumber by a random phase, and then inverse Fourier transforming. This method has also been used in other areas of research. Henceforth I call this the *random-phase method* (RPM). It is computationally inexpensive and produces synthetic turbulence having second-order statistics consistent with the assumed turbulence spectrum. However, the fields created by this method do not necessarily have third- and higher order statistics that are realistic for turbulence. In particular, RPM cannot capture intermittent features known to be characteristic of turbulence. But if one is interested only in calculating means and second-order statistics of the acoustic field, a method for producing synthetic turbulence that is realistic only to second order may be satisfactory. Hence RPM can be useful in certain applications.

One shortcoming of RPM as implemented by Gilbert et al. is that the turbulence model they used was an isotropic, homogeneous Gaussian model.

Atmospheric turbulence, particularly near the ground, is known to violate all these properties. Actually, Gilbert et al.'s method *can* be used to synthesize anisotropic non-Gaussian turbulence. One would simply have to start with the appropriate turbulence model for the spectral density function. It is the inability of the standard RPM to incorporate inhomogeneity that, in the end, limits its utility. Therefore we need a method for generalizing RPM so that inhomogeneous turbulence structure can be synthesized.

In section 3.2, I describe a generalized random-phase method (GRPM) to synthesize turbulence for a given spectral model, be it homogeneous or inhomogeneous. Next, in section 3.3, I show how the method reduces to the RPM used by Gilbert et al. (1990) for homogeneous turbulence. Last, in section 3.4, the method is applied to vertically inhomogeneous turbulence, which is a case of particular interest for the atmosphere.

3.2 Generalized Random-Phase Method

The basic idea underlying GRPM is to multiply the *empirical orthogonal functions* (EOFs) by random phases and then sum them to form the synthetic turbulence field. The reason why this reduces to the standard RPM in the case of homogeneous turbulence is that the EOFs of a homogeneous correlation function are harmonic functions (Lumley, 1971, Wilson, 1996). The EOFs are defined as the eigenfunctions of the correlation function:

$$\int R\left(\mathbf{x},\mathbf{x}'\right)\psi\left(\mathbf{x}'\right)d\mathbf{x}' = \lambda\psi\left(\mathbf{x}\right),$$

where $\mathbf{x} = (x_1, x_2, x_3)$, the ψ's are the EOFs, and λ is the eigenvalue. (Although the above equation was specifically written for the scalar case, it can be used for vector fields as well. The generalization of the eigenvalue problem to vectors and to multiple, correlated fields is accomplished through tensors (e.g., Wilson, 1996).)

Here is a step-by-step description of the GRPM:

1. Fourier transform the eigenvalue problem with respect to the homogeneous coordinates. Because the eigenvalue equation is a convolution with respect to the homogeneous coordinates, the eigenvalue problem is reduced to a simple multiplication after the transform, and we are left only with an integration over the inhomogeneous coordinates (Wilson, 1996). The result is

$$\int \hat{R}\left(\mathbf{k};\boldsymbol{\xi},\boldsymbol{\xi}'\right)\hat{\psi}\left(\mathbf{k};\boldsymbol{\xi}'\right)d\boldsymbol{\xi}' = \lambda\left(\mathbf{k}\right)\hat{\psi}\left(\mathbf{k};\boldsymbol{\xi}\right). \tag{66}$$

   In the above, functions that have been transformed with respect to the homogeneous coordinates are indicated by a "hat," e.g., $\hat{\psi}$. The

inhomogeneous coordinates are indicated by $\boldsymbol{\xi}$, and the wavenumbers corresponding to the homogeneous coordinates are indicated by $\mathbf{k}$.

2. Find the eigenfunctions and eigenvalues in the transformed domain. Let us indicate the solutions as $\hat{\psi}_n(\mathbf{k};\boldsymbol{\xi})$, $\lambda_n(\mathbf{k})$, where $n = 1, 2, 3, \ldots$ The eigenfunctions are orthonormal, so that

$$\int \hat{\psi}_m(\mathbf{k};\boldsymbol{\xi})\,\hat{\psi}_n^*(\mathbf{k};\boldsymbol{\xi})\,d\boldsymbol{\xi} = \delta_{mn}, \tag{67}$$

where $\delta_{mn} = 1$ if $m = n$ and zero otherwise.

3. Expand the transformed, synthetic field $\hat{s}(\mathbf{k};\boldsymbol{\xi})$ in terms of the eigenfunctions $\hat{\psi}_n(\mathbf{k};\boldsymbol{\xi})$:

$$\hat{s}(\mathbf{k};\boldsymbol{\xi}) = \sum_n a_n(\mathbf{k})\,\hat{\psi}_n(\mathbf{k};\boldsymbol{\xi}). \tag{68}$$

Note that the expansion coefficients $a_n(\mathbf{k})$ are random functions.

4. Determine the coefficients in the expansion such that

$$\hat{R}(\mathbf{k};\boldsymbol{\xi},\boldsymbol{\xi}') = \langle \hat{s}(\mathbf{k};\boldsymbol{\xi})\,\hat{s}^*(\mathbf{k};\boldsymbol{\xi}')\rangle. \tag{69}$$

(The asterisk indicates complex conjugation.)

5. Inverse Fourier transform $\hat{s}(\mathbf{k};\boldsymbol{\xi})$ to find $s(\mathbf{x})$.

The key to the procedure is step 4. By selecting the expansion coefficients in this manner, we assure that the correlation function of the synthetic field matches the model correlation function. So, how do we choose the expansion coefficients such that equation (69) is satisfied? First note that by substituting the expansion (68) into (69), we have

$$\hat{R}(\mathbf{k};\boldsymbol{\xi},\boldsymbol{\xi}') = \sum_m \sum_n \langle a_m(\mathbf{k})\,a_n^*(\mathbf{k})\rangle\,\hat{\psi}_m(\mathbf{k};\boldsymbol{\xi})\,\hat{\psi}_n^*(\mathbf{k};\boldsymbol{\xi}').$$

Multiplying both sides by $\hat{\psi}_j(\mathbf{k};\boldsymbol{\xi}')$, integrating with respect to $\boldsymbol{\xi}'$, and invoking orthonormality, we have

$$\int \hat{R}(\mathbf{k};\boldsymbol{\xi},\boldsymbol{\xi}')\,\hat{\psi}_j(\mathbf{k};\boldsymbol{\xi}')\,d\boldsymbol{\xi}' = \sum_m \left\langle a_m(\mathbf{k})\,a_j^*(\mathbf{k})\right\rangle \hat{\psi}_m(\mathbf{k};\boldsymbol{\xi}).$$

Comparison with equation (66) now yields

$$\sum_m \langle a_m(\mathbf{k})\,a_j(\mathbf{k})\rangle\,\hat{\psi}_m(\mathbf{k};\boldsymbol{\xi}) = \lambda_j(\mathbf{k})\,\hat{\psi}_j(\mathbf{k};\boldsymbol{\xi}).$$

Finally, multiplying by $\hat{\psi}_n^*(\mathbf{k};\boldsymbol{\xi})$, integrating, and invoking orthonormality one more time, we find

$$\langle a_m(\mathbf{k})\, a_n^*(\mathbf{k})\rangle = \delta_{mn}\lambda_n(\mathbf{k}). \tag{70}$$

This equation shows that the expansion coefficients are *statistically* orthogonal, and that the expected value of their magnitude squared equals the corresponding eigenvalue. The simplest way to choose the coefficients while satisfying the orthogonality relationship is to set

$$a_n(\mathbf{k}) = \sqrt{\lambda_n(\mathbf{k})}\exp(i\gamma_n(\mathbf{k})), \tag{71}$$

where $\gamma_n(\mathbf{k})$ is some random phase. This method for choosing the coefficients is the basis of GRPM.

3.3 Homogeneous Turbulence

Application of GRPM to homogeneous turbulence is particularly simple. In this case, the Fourier transform is applied to all coordinates, and the transformed eigenvalue problem corresponding to equation (66) is simply

$$\Phi(\boldsymbol{\kappa})\,\hat{\psi}(\boldsymbol{\kappa}) = \lambda(\boldsymbol{\kappa})\,\hat{\psi}(\boldsymbol{\kappa}). \tag{72}$$

We make the eigenfunctions orthonormal by setting $\hat{\psi}(\boldsymbol{\kappa}) = 1$. Hence $\Phi(\boldsymbol{\kappa}) = \lambda(\boldsymbol{\kappa})$, and equation (71) becomes

$$a(\boldsymbol{\kappa}) = \sqrt{\Phi(\boldsymbol{\kappa})}\exp(i\gamma(\boldsymbol{\kappa})). \tag{73}$$

The transformed field is simply $\hat{s}(\boldsymbol{\kappa}) = a(\boldsymbol{\kappa})$.

3.4 Vertically Inhomogeneous Turbulence

The next most complicated case occurs when one of the coordinates is inhomogeneous. This is an important special case, since over relatively flat terrain, atmospheric boundary layer structure is approximately homogeneous in the horizontal directions, but inhomogeneous in the vertical. In this situation, the function $\hat{R}(\mathbf{k};\boldsymbol{\xi},\boldsymbol{\xi}')$ is the 2D cross spectrum, $\phi(\kappa_1,\kappa_2;z,z')$, discussed in section 2.4. The eigenvalue problem is

$$\int \phi(\kappa_1,\kappa_2;z,z')\,\hat{\psi}(\kappa_1,\kappa_2;z')\,dz' = \lambda(\kappa_1,\kappa_2)\,\hat{\psi}(\kappa_1,\kappa_2;z). \tag{74}$$

Generally one must solve the eigenvalue problem by discretizing the computational domain in the z-direction, and then numerically solving the resulting matrix equation (Moin and Moser, 1989, Wilson, 1996). The expansion coefficients are

$$a_n(\kappa_1, \kappa_2) = \sqrt{\lambda_n(\kappa_1, \kappa_2)} \exp\left(i\gamma_n(\kappa_1, \kappa_2)\right), \tag{75}$$

where $n = 1, 2, \ldots, N$, N being the number of grid points in the z-direction.

4. Gaussian Model

4.1 Energy Spectrum and 3D Correlations

Starting with this section, I consider specific statistical models for atmospheric turbulence. Unfortunately, there are no 3D turbulence models that are known to work satisfactorily for a variety of atmospheric conditions. Hence we are forced to consider idealized models.

In this section I consider one such idealization, the Gaussian model. The main advantage of the Gaussian model is its analytical convenience. But it only works well for qualitatively modeling the largest scale features of the turbulence (the energy subrange). The von Kármán model (described in sect. 4.2) is somewhat more general, since it also describes the smaller scale structure (the inertial subrange) realistically.

The energy spectrum, for the scalar Gaussian model, is defined as

$$E_s(\kappa) = \frac{\sigma^2 \kappa^4 L^5}{24\sqrt{\pi}} \exp\left(-\frac{\kappa^2 L^2}{4}\right). \tag{76}$$

In accordance with the discussion in section 2.7, the energy spectrum for the vector Gaussian model is three times the scalar model:

$$E_v(\kappa) = \frac{\sigma^2 \kappa^4 L^5}{8\sqrt{\pi}} \exp\left(-\frac{\kappa^2 L^2}{4}\right). \tag{77}$$

By integration of equation (31), the function $\hat{f}(\kappa)$ can be found from $E_v(\kappa)$. The result for the Gaussian spectrum is

$$\hat{f}(\kappa) = \frac{L}{2\sqrt{\pi}} \exp\left(-\frac{\kappa^2 L^2}{4}\right). \tag{78}$$

The longitudinal correlation function is found by calculation of the inverse Fourier transform:

$$f(r) = \exp\left(-\frac{r^2}{L^2}\right). \tag{79}$$

The lateral correlation function, found by equation (9), is

$$g(r) = \left(1 - \frac{r^2}{L^2}\right) \exp\left(-\frac{r^2}{L^2}\right). \tag{80}$$

Finally, from equation (58), we have the scalar correlation function*

$$h(r) = \left(1 - \frac{2}{3}\frac{r^2}{L^2}\right) \exp\left(-\frac{r^2}{L^2}\right), \tag{81}$$

and its Fourier transform

$$\hat{h}(\kappa) = \frac{L}{3\sqrt{\pi}} \left(1 + \frac{\kappa^2 L^2}{4}\right) \exp\left(-\frac{\kappa^2 L^2}{4}\right). \tag{82}$$

By performing the integration in equation (43), we find

$$\mathcal{L}_{\parallel} = \frac{\sqrt{\pi}}{2} L = 0.886L. \tag{83}$$

Hence, from equation (59),

$$\mathcal{L} = \frac{\sqrt{\pi}}{3} L = 0.591L. \tag{84}$$

The energy spectrum, as a function of $k\mathcal{L}$, is plotted in figure 1.

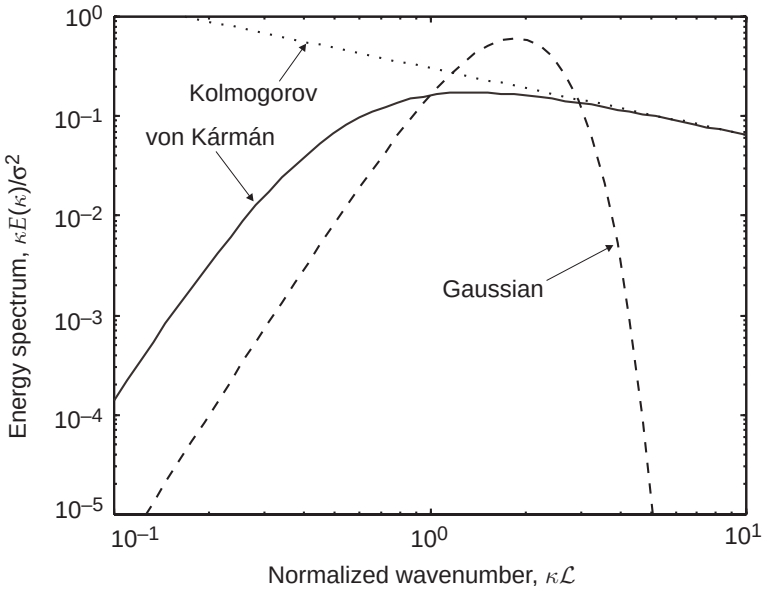

Figure 1. Comparison of energy spectral functions for Gaussian, von Kármán, and Kolmogorov models.

*Previous authors (such as Ostashev, 1994) have used $f(r) = h(r) = \exp\left(-r^2/L^2\right)$. The equation used for $h(r)$ in this report is different because of the "energy spectral approach" I follow. Since neither equation (79) nor (81) is known to agree more satisfactorily with data, it is ultimately a matter of convention which one is used.

4.2 1D Cross Spectra

The 1D cross spectrum can be found by calculation of the Fourier transform of the correlation function with respect to r_1. The required integrals are given by equations (3.896.4) and (3.952.4) in Gradshteyn and Ryzhik (1994). For scalars, one finds

$$\Theta\left(\kappa; r_2, r_3\right) = \frac{\sigma^2 L}{3\sqrt{\pi}} \left(1 - \frac{r_\perp^2}{L^2} + \frac{\kappa^2 L^2}{4}\right) \exp\left(-\frac{\kappa^2 L^2}{4} - \frac{r_\perp^2}{L^2}\right), \qquad (85)$$

where $r_\perp^2 = r_2^2 + r_3^2$. The results for vectors are similarly found to be

$$\Theta_{11}\left(\kappa; r_2, r_3\right) = \frac{\sigma^2 L}{2\sqrt{\pi}} \left(1 - \frac{r_\perp^2}{L^2}\right) \exp\left(-\frac{\kappa^2 L^2}{4} - \frac{r_\perp^2}{L^2}\right), \quad \text{and} \qquad (86)$$

$$\Theta_{22}\left(\kappa; r_2, r_3\right) = \frac{\sigma^2 L}{4\sqrt{\pi}} \left(1 - \frac{2r_3^2}{L^2} + \frac{\kappa^2 L^2}{2}\right) \exp\left(-\frac{\kappa^2 L^2}{4} - \frac{r_\perp^2}{L^2}\right). \qquad (87)$$

The equation for $\Theta_{33}\left(\kappa; r_2, r_3\right)$ is the same as the one for $\Theta_{22}\left(\kappa; r_2, r_3\right)$, except that r_2 replaces r_3 on the right.

4.3 2D Correlation Function

The scalar 2D correlation function can be found from the energy spectrum by substitution of equation (76) into (22):

$$b(\rho) = \frac{\sigma^2 L}{3\sqrt{\pi}} \int_0^\infty \kappa^3 \exp\left(-\frac{\kappa^2 L^2}{4}\right) J_0\left(\kappa\rho\right)\, d\kappa.$$

The solution to this integral, from equation (11.4.28) in Abramowitz and Stegun (1965), is

$$b(\rho) = \frac{\sigma^2 L}{3\sqrt{\pi}} M\left(2, 1, -\frac{\rho^2}{L^2}\right),$$

where $M()$ is called Kummer's function. From (13.4.1) and (13.6.12) in Abramowitz and Stegun (1965), we see that $M\left(2,1,z\right) = \left(1+z\right) \times M\left(1,1,z\right) = \left(1+z\right)e^z$. Hence our result for the 2D correlation function is

$$b(\rho) = \frac{\sigma^2 L}{3\sqrt{\pi}} \left(1 - \frac{\rho^2}{L^2}\right) \exp\left(-\frac{\rho^2}{L^2}\right). \qquad (88)$$

An equation equivalent to this one was given previously by Mellert et al. (1994). The 2D correlation function for the velocity field $b_{\|}(\rho)$ is found simply by multiplication by $3/2$, as indicated by equation (63).

The 2D structure function for the Gaussian model,

$$d(\rho) = 2\left[b(\rho) - b(0)\right] = \frac{2\sigma^2 L}{3\sqrt{\pi}}\left[1 - \left(1 - \frac{\rho^2}{L^2}\right)\exp\left(-\frac{\rho^2}{L^2}\right)\right], \tag{89}$$

is plotted in figure 2.

4.4 2D and 3D Spectra

The 2D spectrum for a Gaussian scalar can be found without much difficulty through the integration in equation (35). The result is

$$\phi(\kappa_h) = \frac{\sigma^2 L^2}{12\pi}\left(1 + \frac{\kappa_h^2 L^2}{2}\right)\exp\left(-\frac{\kappa_h^2 L^2}{4}\right). \tag{90}$$

Similarly, we find for vectors

$$\phi_{11}(\kappa_1, \kappa_2) = \frac{\sigma^2 L^2}{8\pi}\left(1 + \frac{\kappa_1^2 L^2}{2}\right)\exp\left(-\frac{\kappa_h^2 L^2}{4}\right), \quad \text{and} \tag{91}$$

$$\phi_{33}(\kappa_h) = \frac{\sigma^2 \kappa_h^2 L^4}{16\pi}\exp\left(-\frac{\kappa_h^2 L^2}{4}\right). \tag{92}$$

The 3D spectra are computed easily from the energy spectrum (eq (76) and (77)), with equation (12) used for scalars and equation (16) for vectors.

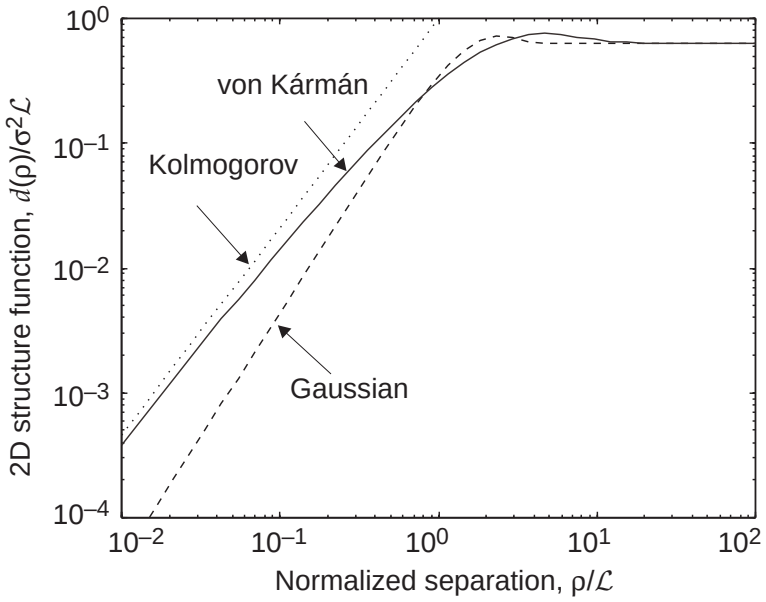

Figure 2. Comparison of 2D structure functions corresponding to Gaussian, von Kármán, and Kolmogorov turbulence models.

4.5 2D Cross Spectra

One can find the 2D cross spectrum by calculating the inverse Fourier transform of the 3D spectra with respect to κ_3. For scalars, the resulting integrals are calculated with equations (3.896.4) and (3.952.4) from Gradshteyn and Ryzhik (1994). The result is

$$\phi\left(\kappa_1, \kappa_2; r_3\right) = \frac{\sigma^2 L^2}{12\pi}\left(1 - \frac{2r_3^2}{L^2} + \frac{\kappa_h^2 L^2}{2}\right)\exp\left(-\frac{\kappa_h^2 L^2}{4} - \frac{r_3^2}{L^2}\right). \tag{93}$$

The corresponding equations for vectors are

$$\phi_{11}\left(\kappa_1, \kappa_2; r_3\right) = \frac{\sigma^2 L^2}{8\pi}\left(1 - \frac{2r_3^2}{L^2} + \frac{\kappa_2^2 L^2}{2}\right)\exp\left(-\frac{\kappa_h^2 L^2}{4} - \frac{r_3^2}{L^2}\right), \quad \text{and} \tag{94}$$

$$\phi_{33}\left(\kappa_1, \kappa_2; r_3\right) = \frac{\sigma^2 \kappa_h^2 L^4}{16\pi}\exp\left(-\frac{\kappa_h^2 L^2}{4} - \frac{r_3^2}{L^2}\right). \tag{95}$$

The equation for $\phi_{22}\left(\kappa_1, \kappa_2; r_3\right)$ is the same as equation (94), except that κ_2 on the right side is replaced by κ_1.

5. Von Kármán Model

5.1 Model Definition and Energy Spectrum

The von Kármán model is developed from the following equation for the energy spectrum of a scalar:

$$E_s(\kappa) = \frac{4\Gamma(\nu+5/2)}{3\sqrt{\pi}\Gamma(\nu)} \frac{\sigma^2\kappa^4\ell^5}{(1+\kappa^2\ell^2)^{\nu+5/2}}. \tag{96}$$

The parameter ℓ is a characteristic length scale, $\Gamma()$ is the gamma function, and ν controls the power-law dependence in the inertial subrange ($\kappa\ell \gg 1$). Generally, we set $\nu = 1/3$ to obtain Kolmogorov's (1941) $\kappa^{-5/3}$ power law for the inertial subrange. Figure 1 (p 24) compares the von Kármán energy spectrum to the Gaussian energy spectrum. The main difference between the von Kármán and Gaussian models is that the Gaussian model decays much more rapidly at large wavenumbers. The vector von Kármán energy spectrum is simply three times the scalar one, so that equation (15) is satisfied.

Complete results for the vector version of the von Kármán model were given previously (Wilson, 1997b). With these vector results as a starting point, the equations in section 2.7 allow us to find the corresponding scalar results with little difficulty. For completeness, I provide here the important results for both scalars and vectors:

$$h(r) = \frac{2}{\Gamma(1/3)}\left(\frac{r}{2\ell}\right)^{1/3}\left[K_{1/3}\left(\frac{r}{\ell}\right) - \left(\frac{r}{3\ell}\right)K_{2/3}\left(\frac{r}{\ell}\right)\right], \tag{97}$$

$$\hat{h}(\kappa) = \frac{\Gamma(5/6)}{9\sqrt{\pi}\Gamma(1/3)} \frac{\ell}{(1+\kappa^2\ell^2)^{5/6}}\left[11 - \frac{5}{1+\kappa^2\ell^2}\right], \tag{98}$$

$$f(r) = \frac{2}{\Gamma(1/3)}\left(\frac{r}{2\ell}\right)^{1/3} K_{1/3}\left(\frac{r}{\ell}\right), \tag{99}$$

$$\hat{f}(\kappa) = \frac{\Gamma(5/6)}{\sqrt{\pi}\Gamma(1/3)} \frac{\ell}{(1+\kappa^2\ell^2)^{5/6}}, \tag{100}$$

$$g(r) = \frac{2}{\Gamma(1/3)}\left(\frac{r}{2\ell}\right)^{1/3}\left[K_{1/3}\left(\frac{r}{\ell}\right) - \left(\frac{r}{2\ell}\right)K_{2/3}\left(\frac{r}{\ell}\right)\right], \quad \text{and} \tag{101}$$

$$\widehat{g}(\kappa) = \frac{\Gamma(5/6)}{\sqrt{\pi}\Gamma(1/3)} \frac{\ell}{(1+\kappa^2\ell^2)^{5/6}}\left[\frac{4}{3} - \frac{5}{6(1+\kappa^2\ell^2)}\right], \tag{102}$$

where K_ν is the modified Bessel function of the second kind.

The integral length scales are

$$\mathcal{L} = \frac{2\sqrt{\pi}\Gamma(5/6)}{3\Gamma(1/3)}\ell = 0.498\ell \quad \text{and} \tag{103}$$

$$\mathcal{L}_\parallel = \frac{\sqrt{\pi}\Gamma(5/6)}{\Gamma(1/3)}\ell = 0.747\ell. \tag{104}$$

5.2 1D Cross Spectra

Equations for the vector 1D cross spectra were derived previously (Wilson, 1997b). The results are

$$\Theta_{11}(\kappa; r_2, r_3) = \frac{2\sigma^2\ell}{\sqrt{\pi}\Gamma(1/3)}\left(\frac{\xi/2}{1+\kappa^2\ell^2}\right)^{5/6}\left[K_{5/6}(\xi) - \frac{\xi}{2}K_{1/6}(\xi)\right], \quad \text{and} \tag{105}$$

$$\Theta_{22}(\kappa; r_2, r_3) = \frac{2\sigma^2\ell}{\sqrt{\pi}\Gamma(1/3)}\left(\frac{\xi/2}{1+\kappa^2\ell^2}\right)^{5/6} \times\left[\frac{4}{3}K_{5/6}(\xi) - \frac{\xi/2}{1+\kappa^2\ell^2}K_{11/6}(\xi) + \frac{r_2^2(1+\kappa^2\ell^2)}{2\xi\ell^2}K_{1/6}(\xi)\right], \tag{106}$$

where $\xi^2 = (r_2^2 + r_3^2)(1+\kappa^2\ell^2)/\ell^2$. The equation for $\Theta_{33}(\kappa; r_2, r_3)$ is the same as the preceding, except that r_3 replaces r_2 on the right. The scalar result follows from equation (62):

$$\Theta(\kappa; r_2, r_3) = \frac{2\sigma^2\ell}{3\sqrt{\pi}\Gamma(1/3)}\left(\frac{\xi/2}{1+\kappa^2\ell^2}\right)^{5/6}\left[\frac{11}{3}K_{5/6}(\xi) - \frac{\xi}{1+\kappa^2\ell^2}K_{11/6}(\xi)\right]. \tag{107}$$

5.3 2D Correlation Function

The 2D correlation function for the scalar von Kármán model is

$$b(\rho) = \frac{4\sigma^2\ell}{3\sqrt{\pi}\Gamma(1/3)}\left(\frac{\rho}{2\ell}\right)^{5/6}\left[K_{5/6}\left(\frac{\rho}{\ell}\right) - \frac{\rho}{2\ell}K_{1/6}\left(\frac{\rho}{\ell}\right)\right]. \tag{108}$$

Integrals (3.773.6) and (6.726.4) in Gradshteyn and Rhyzhik (1994) were used to derive this result. As before, the vector 2D correlation function $b_\parallel(\rho)$ is simply $3/2$ times the scalar result. The 2D structure function for the scalar von Kármán model is plotted and compared to the Gaussian model in figure 2 (p 26).

5.4 2D and 3D Spectra

The 2D spectra for the vector von Kármán model, derived elsewhere (Wilson, 1997b), are

$$\phi_{11}(\kappa_1,\kappa_2) = \frac{\sigma^2\ell^2}{6\pi\left(1+\kappa_h^2\ell^2\right)^{4/3}}\left[1+\frac{8}{3}\frac{\kappa_2^2\ell^2}{1+\kappa_h^2\ell^2}\right], \tag{109}$$

$$\phi_{33}(\kappa_1,\kappa_2) = \frac{4\sigma^2\kappa_h^2\ell^4}{9\pi\left(1+\kappa_h^2\ell^2\right)^{7/3}}, \tag{110}$$

$$\phi_{12}(\kappa_1,\kappa_2) = -\frac{4\sigma^2\kappa_1\kappa_2\ell^4}{9\pi\left(1+\kappa_h^2\ell^2\right)^{7/3}}, \quad \text{and} \tag{111}$$

$$\phi_{13}(\kappa_1,\kappa_2) = 0. \tag{112}$$

The scalar 2D spectrum, found with equation (64), is

$$\phi(\kappa_h) = \frac{\sigma^2\ell^2}{9\pi\left(1+\kappa_h^2\ell^2\right)^{4/3}}\left[1+\frac{8}{3}\frac{\kappa_h^2\ell^2}{1+\kappa_h^2\ell^2}\right]. \tag{113}$$

The 3D spectra are computed easily from the energy spectrum, equation (96), with equation (12) used for scalars and (16) for vectors.

5.5 2D Cross Spectra

The 2D cross spectra for the vector von Kármán model are (Wilson, 1997b)

$$\begin{aligned}\phi_{11}(\kappa_1,\kappa_2;r_3) &= \frac{2\sigma^2\ell^2\left(\zeta_h/2\right)^{4/3}}{\pi\Gamma\left(1/3\right)\left(1+\kappa_h^2\ell^2\right)^{4/3}} \\ &\quad\times\left[\frac{11}{6}K_{4/3}(\zeta_h)-\frac{\zeta_h(1+\kappa_1^2\ell^2)}{2(1+\kappa_h^2\ell^2)}K_{7/3}(\zeta_h)\right],\end{aligned} \tag{114}$$

$$\phi_{33}(\kappa_1,\kappa_2;r_3) = \frac{2\sigma^2\kappa_h^2\ell^4\left(\zeta_h/2\right)^{7/3}}{\pi\Gamma\left(1/3\right)\left(1+\kappa_h^2\ell^2\right)^{7/3}}K_{7/3}(\zeta_h), \tag{115}$$

where $\zeta_h = (r_3/\ell)\sqrt{1+\kappa_h^2\ell^2}$. The equation for ϕ_{22} is the same as the one for ϕ_{11}, except that κ_2 replaces κ_1 on the right. The scalar 2D cross spectrum, found from equation (64), is

$$\begin{aligned}\phi(\kappa_1,\kappa_2;r_3) &= \frac{4\sigma^2\ell^2\left(\zeta_h/2\right)^{4/3}}{3\pi\Gamma\left(1/3\right)\left(1+\kappa_h^2\ell^2\right)^{4/3}} \\ &\quad\times\left[\frac{11}{6}K_{4/3}(\zeta_h)-\frac{\zeta_h}{2(1+\kappa_h^2\ell^2)}K_{7/3}(\zeta_h)\right].\end{aligned} \tag{116}$$

6. Kolmogorov Model

6.1 Energy Spectrum and Model Definition

The Kolmogorov model is based on scaling hypotheses that apply only to the inertial subrange: that is, for $\rho \ll \mathcal{L}$ in the spatial domain, or $\kappa\mathcal{L} \gg 1$ in the wavenumber domain. Actually, the von Kármán model discussed in the previous section has an inertial subrange satisfying Kolmogorov's hypotheses. Therefore the approach I take for deriving the Kolmogorov model is simply to calculate limiting forms of the von Kármán model. It needs to be pointed out, though, that this procedure produces a *possible* Kolmogorov model; there is no *unique* Kolmogorov model. Kolmogorov's hypotheses provide only proportionality relations; the numerical constants appearing in the equations in this section depend in part on assumptions intrinsic to the von Kármán model.

The energy spectrum for scalars is the large $\kappa\ell$-limit of equation (96):

$$E_s(\kappa) = \frac{4\Gamma(17/6)}{3\sqrt{\pi}\Gamma(1/3)}\sigma^2\ell(\kappa\ell)^{-5/3}. \tag{117}$$

(Since ℓ and $\mathcal{L}$ are the same order, $\kappa\mathcal{L} \gg 1$ is equivalent to $\kappa\ell \gg 1$.) This scalar energy spectrum is plotted in figure 1. As before, we choose $E_v(\kappa) = 3E_s(\kappa)$. In the next section, I derive expressions for the structure-function parameters (defined later in eq (130) and (131)). These enable us to write the energy spectra as

$$E_s(\kappa) = \frac{2^{5/3}}{11\sqrt{\pi}}\frac{\Gamma(17/6)}{\Gamma(2/3)}C_s^2\kappa^{-5/3} \simeq 0.2074C_s^2\kappa^{-5/3}, \quad \text{and} \tag{118}$$

$$E_v(\kappa) = \frac{2^{5/3}}{3\sqrt{\pi}}\frac{\Gamma(17/6)}{\Gamma(2/3)}C_v^2\kappa^{-5/3} \simeq 0.7604C_v^2\kappa^{-5/3}. \tag{119}$$

Equations (118) and (119) (but not eq (117)) are the ones that would normally be used for the Kolmogorov model. The reason is that equation (117) explicitly contains σ^2 and ℓ, two parameters that depend primarily on the large-scale structure of the flow. On the other hand, equations (118) and

(119) contain structure-function parameters, which describe the small-scale (inertial subrange) structure of the flow.*

For the 1D spectra, we find

$$\hat{h}(\kappa) = \frac{11\Gamma(5/6)}{9\sqrt{\pi}\Gamma(1/3)}\ell(\kappa\ell)^{-5/3}, \quad \text{and} \tag{120}$$

$$\hat{f}(\kappa) = \frac{\Gamma(5/6)}{\sqrt{\pi}\Gamma(1/3)}\ell(\kappa\ell)^{-5/3}. \tag{121}$$

In terms of the structure-function parameter, the 1D scalar spectrum is

$$\sigma^2\hat{h}(\kappa) = \frac{\Gamma(5/6)\,2^{2/3}}{6\sqrt{\pi}\Gamma(2/3)}C_s^2\kappa^{-5/3} \simeq 0.1244C_s^2\kappa^{-5/3}. \tag{122}$$

The equation for the 1D longitudinal vector spectrum is the same as equation (122), except with C_v^2 replacing C_s^2. The 1D transverse spectrum is $4/3$ times the longitudinal spectrum.

---

*The Kolmogorov spectral equations given by Tatarskii (1971) and Ostashev (1994) differ somewhat from equations (118) and (119). For example, the 3D spectral density of a scalar is given as

$$\Phi(\kappa) = \frac{5\sqrt{3}\Gamma(2/3)}{36\pi^2}C_s^2\kappa^{-11/3}. \tag{a}$$

On the other hand, since $\Phi(\kappa) = E_s(\kappa)/2\pi\kappa^2$, equation (118) implies

$$\Phi(\kappa) = \frac{2^{2/3}}{11\pi^{3/2}}\frac{\Gamma(17/6)}{\Gamma(2/3)}C_s^2\kappa^{-11/3}. \tag{b}$$

To prove that this equation is equivalent to the one given by Tatarskii and Ostashev, we first use the recursion property of the gamma function, $\Gamma(z+1) = z\Gamma(z)$. Hence,

$$\Gamma\left(\frac{17}{6}\right) = \frac{55}{36}\Gamma\left(\frac{5}{6}\right).$$

From the duplication formula for the gamma function (eq (6.1.18) in Abramowitz & Stegun, 1965), we have

$$\Gamma\left(\frac{2}{3}\right) = \frac{1}{2^{1/3}\sqrt{\pi}}\Gamma\left(\frac{1}{3}\right)\Gamma\left(\frac{5}{6}\right).$$

Furthermore, from the reflection formula (eq (6.1.17) in Abramowitz & Stegun, 1965),

$$\Gamma\left(\frac{1}{3}\right)\Gamma\left(\frac{2}{3}\right) = \frac{2\pi}{\sqrt{3}}.$$

Putting these various results together, we find

$$\frac{\Gamma(17/6)}{\Gamma(2/3)} = \frac{55}{36}\frac{\sqrt{3}}{2^{2/3}\sqrt{\pi}}\Gamma\left(\frac{2}{3}\right).$$

Tatarskii and Ostashev's equation (a) follows immediately upon substitution of this result into equation (b).

To find the limiting forms of the correlations for small r/ℓ, the following expansion of the Bessel functions for small arguments can be used:

$$K_\nu(\xi) \simeq \frac{\Gamma(\nu)}{2}\left(\frac{\xi}{2}\right)^{-\nu} - \frac{\Gamma(1-\nu)}{2\nu}\left(\frac{\xi}{2}\right)^{\nu}. \tag{123}$$

Note that $f(r)$, $g(r)$, and $h(r)$ in the von Kármán model all have the form

$$\varphi(r) = \frac{2}{\Gamma(1/3)}\left(\frac{r}{2\ell}\right)^{1/3}\left[K_{1/3}\left(\frac{r}{\ell}\right) - a\left(\frac{r}{\ell}\right)K_{2/3}\left(\frac{r}{\ell}\right)\right], \tag{124}$$

where $a = 0$ for $f(r)$, $a = 1/2$ for $g(r)$, and $a = 1/3$ for $h(r)$. For the inertial subrange, then, the general result is

$$\varphi(r) = 1 - (3+2a)\frac{\Gamma(2/3)}{\Gamma(1/3)}\left(\frac{r}{2\ell}\right)^{2/3}. \tag{125}$$

6.2 Structure Functions and Parameters

The structure functions are found by substitution of equation (125) into equations (49), (51), and (52). The results are

$$D(r) = \frac{22\Gamma(2/3)}{3\Gamma(1/3)}\left(\frac{r}{2\ell}\right)^{2/3}, \tag{126}$$

$$D_\parallel(r) = \frac{6\sigma^2\Gamma(2/3)}{\Gamma(1/3)}\left(\frac{r}{2\ell}\right)^{2/3}, \quad \text{and} \tag{127}$$

$$D_\perp(r) = \frac{8\sigma^2\Gamma(2/3)}{\Gamma(1/3)}\left(\frac{r}{2\ell}\right)^{2/3}. \tag{128}$$

Using equations (10) and (50), we have more generally for the velocity fluctuations

$$D_{\alpha\alpha}(r) = \frac{2\sigma^2\Gamma(2/3)}{\Gamma(1/3)}\left(\frac{r}{2\ell}\right)^{2/3}\left(4 - \frac{r_\alpha^2}{r^2}\right). \tag{129}$$

The structure-function parameter is defined as the ratio $D(r)/r^{2/3}$ for small r. Hence the structure-function parameter for scalars is

$$C_s^2 = \frac{22\sigma^2\Gamma(2/3)}{3\Gamma(1/3)}\left(\frac{1}{2\ell}\right)^{2/3} \simeq 2.335\sigma^2\ell^{-2/3}, \tag{130}$$

and for vectors

$$C_v^2 = \frac{6\sigma^2\Gamma(2/3)}{\Gamma(1/3)}\left(\frac{1}{2\ell}\right)^{2/3} \simeq 1.911\sigma^2\ell^{-2/3}. \tag{131}$$

Therefore equation (129) can be rewritten as

$$D_{\alpha\alpha}(r) = \frac{C_v^2}{3} r^{2/3} \left(4 - \cos^2\alpha\right) = C_v^2 r^{2/3} \left[1 + (1/3)\sin^2\alpha\right], \tag{132}$$

where $\cos\alpha = r_\alpha / r$.

For small separations, the scalar 2D correlation function is

$$b(\rho) = \frac{2\sigma^2 \ell \Gamma(5/6)}{3\sqrt{\pi}\Gamma(1/3)} \left[1 - \frac{11}{5}\frac{\Gamma(1/6)}{\Gamma(5/6)}\left(\frac{\rho}{2\ell}\right)^{5/3}\right]. \tag{133}$$

The 2D structure function is hence

$$d(\rho) = 2\left[b(0) - b(\rho)\right] = \frac{44}{15}\frac{\sigma^2 \ell \Gamma(1/6)}{\sqrt{\pi}\Gamma(1/3)}\left(\frac{\rho}{2\ell}\right)^{5/3} \simeq 2.143\sigma^2 \ell^{-2/3}\rho^{5/3}. \tag{134}$$

For vectors,

$$d_\parallel(\rho) = \frac{3}{2} d(\rho) \simeq 3.214\sigma^2 \ell^{-2/3}\rho^{5/3}. \tag{135}$$

In terms of the structure-function parameters, we can write

$$d(\rho) = \frac{1}{5}\frac{\Gamma(1/6)}{\sqrt{\pi}\Gamma(2/3)} C_s^2 \rho^{5/3} \simeq 0.4638 C_s^2 \rho^{5/3}, \quad \text{and} \tag{136}$$

$$d_\parallel(\rho) = \frac{11}{30}\frac{\Gamma(1/6)}{\sqrt{\pi}\Gamma(2/3)} C_v^2 \rho^{5/3} \simeq 0.8504 C_v^2 \rho^{5/3}. \tag{137}$$

Equation (136) is plotted in figure 2 (p 26).

7. HGW Model

The HGW model is essentially a von Kármán model, modified to account for the *blocking* effect of the ground on the turbulence. As a result of ground blocking, the vertical velocity of an eddy must vanish at ground level. This causes the turbulent velocity statistics to be statistically inhomogeneous in the vertical direction. Since I describe the HGW model in detail elsewhere (Wilson, 1997b), here I only summarize the main results, and show how they can be used for wave scattering calculations and random field synthesis.

In previous sections, orientation of the coordinate system was arbitrary. Because the HGW model is anisotropic, we must be specific in this section by using x_3 (that is, z) for the vertical axis.

The basis of the HGW model is the following equation for the 2D cross spectrum of the turbulence:

$$\begin{aligned}\phi_{ij}\left(\kappa_1,\kappa_2;z,z'\right) &= \phi_{ij}^{(H)}\left(\kappa_1,\kappa_2;\left|z'-z\right|\right) \\ &\quad + e^{-\kappa_h z'} m_j\left(\kappa_1,\kappa_2\right)\phi_{3i}^{(H)*}\left(\kappa_1,\kappa_2;z\right) \\ &\quad + e^{-\kappa_h z} m_i^*\left(\kappa_1,\kappa_2\right)\phi_{3j}^{(H)}\left(\kappa_1,\kappa_2;z'\right) \\ &\quad + e^{-\kappa_h (z+z')} m_i^*\left(\kappa_1,\kappa_2\right) m_j\left(\kappa_1,\kappa_2\right)\phi_{33}^{(H)}\left(\kappa_1,\kappa_2;0\right),\end{aligned} \tag{138}$$

where

$$m_j\left(\kappa_1,\kappa_2\right) = \begin{cases} i\kappa_j/\kappa_h, \ j=1 \text{ or } j=2 \\ -1, \ j=3 \end{cases}. \tag{139}$$

The superscripted "(H)" in the equations above means the homogeneous spectrum: that is, the spectrum that would be measured if the boundary (ground) were not present. When the third argument of $\phi_{ij}^{(H)}\left(\kappa_1,\kappa_2;r_3\right)$ is zero, the 2D cross spectrum becomes the ordinary 2D spectrum, so that equations (109) to (112) can be used. For nonzero argument, the following results from Wilson (1997b) are needed in addition to equations (114) and (115):

$$\phi_{12}^{(H)}\left(\kappa_1,\kappa_2;r_3\right) = -\frac{2\sigma^2\kappa_1\kappa_2\ell^4\left(\zeta_h/2\right)^{7/3}}{\pi\Gamma\left(1/3\right)\left(1+\kappa_h^2\ell^2\right)^{7/3}}K_{7/3}\left(\zeta_h\right), \quad \text{and} \tag{140}$$

$$\phi_{13}^{(H)}\left(\kappa_1,\kappa_2;r_3\right) = -\frac{2i\sigma^2\kappa_1\ell^3\left(\zeta_h/2\right)^{7/3}}{\pi\Gamma\left(1/3\right)\left(1+\kappa_h^2\ell^2\right)^{11/6}}K_{4/3}\left(\zeta_h\right). \tag{141}$$

The main difficulty in applying the HGW model is that equation (138) cannot be Fourier transformed analytically. One is therefore forced to use numerical methods.

7.1 1D Cross Spectra

The 1D cross spectra must be calculated numerically. They are very useful for synthesizing turbulence in a vertical plane. As an example, suppose we wish to synthesize the u_1 velocity component in the (x_1, x_3)-plane. The EOFs required by the GRPM are the eigenfunctions of the 3D correlation function $R_{11}(r_1, 0, z, z')$. We can calculate this function by taking the 2D inverse Fourier transform of equation (138) with $i = j = 1$, and evaluate it at $r_2 = 0$. The next step is to Fourier transform the correlation function with respect to the homogeneous coordinates, in this case r_1. The resulting function is the 1D cross spectrum $\Theta_{11}(\kappa_1; 0, z, z')$. It is easily shown that

$$\begin{aligned}\Theta_{11}(\kappa_1; 0, z, z') &= \frac{1}{2\pi}\int_{-\infty}^{\infty} R_{11}(r_1, 0, z, z')\exp(-i\kappa_1 r_1)\, dr_1 \\ &= \int_{-\infty}^{\infty} \phi_{11}(\kappa_1, \kappa_2; z, z')\, d\kappa_2. \end{aligned} \tag{142}$$

The second form is more useful, since it allows Θ_{11} to be determined from a simple 1D integration of ϕ_{11}, which is known from equation (138). Hence for synthesis in a vertical plane, the 1D cross spectral function $\Theta_{11}(\kappa_1; 0, z, z')$ plays the role of $\hat{R}$ in the procedure described in section 3.2. Furthermore, $\mathbf{k} \to \kappa_1$, and $\boldsymbol{\xi} \to z$. Once these identifications are made, it is straightforward to apply the GRPM.

7.2 2D Correlation Function

For homogeneous turbulence, the 2D correlation function can be determined from either equation (20) or (21). Because the 3D spectrum in equation (20) is undefined in inhomogeneous turbulence, however, equation (21) is the only definition directly compatible with the HGW model.

Let us consider the calculation of $b_{\parallel}$, for which the integration and velocity components are aligned. Using the x_1-axis for the direction of propagation, we have

$$b_{\parallel}(r_2, z, z') = \frac{1}{2\pi}\int_{-\infty}^{\infty} R_{11}(r_1, r_2, z, z')\, dr_1. \tag{143}$$

Equivalently, from the Fourier transform definition, equation (4), one has

$$b_{\parallel}(r_2, z, z') = \int_{-\infty}^{\infty} \phi_{11}(0, \kappa_2; z, z')\exp(i\kappa_2 r_2)\, d\kappa_2. \tag{144}$$

Because $m_1(0, \kappa_2) = 0$, only the first term in equation (138), representing the contribution to the spectrum that is unaffected by the ground, is nonzero. Therefore the 2D correlation function for the HGW model is the same as the von Kármán model, equation (108).

7.3 2D and 3D Spectra

It is a simple matter to obtain the 2D spectrum in a horizontal plane for the HGW model: one just sets $z = z'$ in equation (138). On the other hand, the 2D spectra in vertical planes and the 3D spectrum are undefined because of vertical inhomogeneity.

8. Mann Model

The Mann model is the result of applying *rapid distortion theory* to a constant shear layer. The main idea underlying rapid distortion theory is that the shear distortions to an eddy occurring over short time intervals can be modeled by linearized Navier-Stokes equations. Although a full discussion of rapid distortion theory and Mann's model is beyond the scope of this report, the relevant equations are summarized here.

Mann's equations for the 3D autospectra in a uniform (constant gradient) shear layer are

$$\Phi_{11}(\mathbf{k}) = \frac{E(k_0)}{4\pi k_0^4}\left[k_0^2 - k_1^2 - 2k_1 k_{30}\zeta_1 + \left(k_1^2 + k_2^2\right)\zeta_1^2\right], \tag{145}$$

$$\Phi_{22}(\mathbf{k}) = \frac{E(k_0)}{4\pi k_0^4}\left[k_0^2 - k_2^2 - 2k_2 k_{30}\zeta_2 + \left(k_1^2 + k_2^2\right)\zeta_2^2\right], \quad \text{and} \tag{146}$$

$$\Phi_{33}(\mathbf{k}) = \frac{E(k_0)}{4\pi k^4}\left(k_1^2 + k_2^2\right). \tag{147}$$

In the equations above, $E(k_0)$ is the *initial* (before the onset of shear distortion) energy spectrum. The isotropic vector von Kármán energy spectrum is used for $E(k_0)$. The initial wavenumber is $\mathbf{k}_0 = (k_1, k_2, k_{30})$, where $k_{30} = k_3 - \beta k_1$, and β is called the *nondimensional eddy lifetime*. It is given by (Mann, 1994, Wilson, 1998)

$$\beta = \frac{\sqrt{3}\Gamma}{k\ell}\left[B_{1/(1+k^2\ell^2)}\left(\frac{1}{3}, \frac{5}{2}\right)\right]^{-1/2}. \tag{148}$$

The ζ_i are given by the equations

$$\zeta_1 = C_1 - \frac{k_2}{k_1}C_2, \quad \zeta_2 = \frac{k_2}{k_1}C_1 + C_2, \tag{149}$$

where

$$C_1 = \frac{\beta k_1^2\left(k_0^2 - 2k_{30}^2 + \beta k_1 k_{30}\right)}{k^2\left(k_1^2 + k_2^2\right)}, \quad \text{and} \tag{150}$$

$$C_2 = \frac{k_2 k_0^2}{\left(k_1^2 + k_2^2\right)^{3/2}}\arctan\left[\frac{\beta k_1\left(k_1^2 + k_2^2\right)^{1/2}}{k_0^2 - \beta k_{30} k_1}\right]. \tag{151}$$

9. Examples of Synthesized Random Turbulence

I provide here some examples of synthesized turbulence fields, generated by the various turbulence models discussed in previous sections.

9.1 Large-Scale (Buoyantly Driven) Turbulence

The turbulence parameters chosen for this set of examples are intended to be characteristic of the large eddies generated by buoyancy instabilities, such as occur when the sun heats the ground during the day. Specifically, the parameter values for the HGW model are those suggested by Wilson (1997b): $\sigma^2 = 0.35 w_*^2$, where w_*^2 is called the *mixed-layer velocity scale* (Deardorff, 1970a), and $\ell = 0.23 z_i$, where z_i is the boundary-layer inversion height. Besides the HGW model, the models used to make the synthesized fields for this case are the homogeneous von Kármán (sect. 5) and Gaussian (sect. 4) models. The parameters used in the von Kármán model are the same as in the HGW model. For the Gaussian model, $\sigma^2 = 0.35 w_*^2$ and $L = 2\Gamma\left(5/6\right)/\Gamma\left(1/3\right)\ell = 0.194 z_i$ were used. The reason for choosing this value of L is that it results in matching integral length scales for the von Kármán and Gaussian models, as is evident from a comparison of equations (83) and (104).

Figures 3 to 5 show the Gaussian, von Kármán, and HGW models, respectively. All the figures depict vertical planes. The field synthesized is the in-plane horizontal velocity component. The resolution of the simulated fields is 150 grid points in the vertical direction and 200 in the horizontal. The Gaussian field was computed in just a few minutes on a Sun UltraSparc workstation; the von Kármán field required several hours, mainly because of the Bessel function evaluations; and the HGW field required several days, because of the numerical integration to determine the 1D cross spectrum from the 2D cross spectrum. In general, most of the computation time involves determining the 1D cross spectra; the eigenanalysis to determine the EOFs is fast, as is application of the GRPM. Because all three models have axial symmetry, the azimuthal orientation of the vertical plane relative to the wind direction plays no role. The 1D cross spectra (eq (86) and (105) with $r_2 = 0$, and eq (142)) were used to synthesize the fields.

Figure 3. Synthesized turbulent velocity field for buoyantly driven turbulence, generated by a homogeneous Gaussian model.

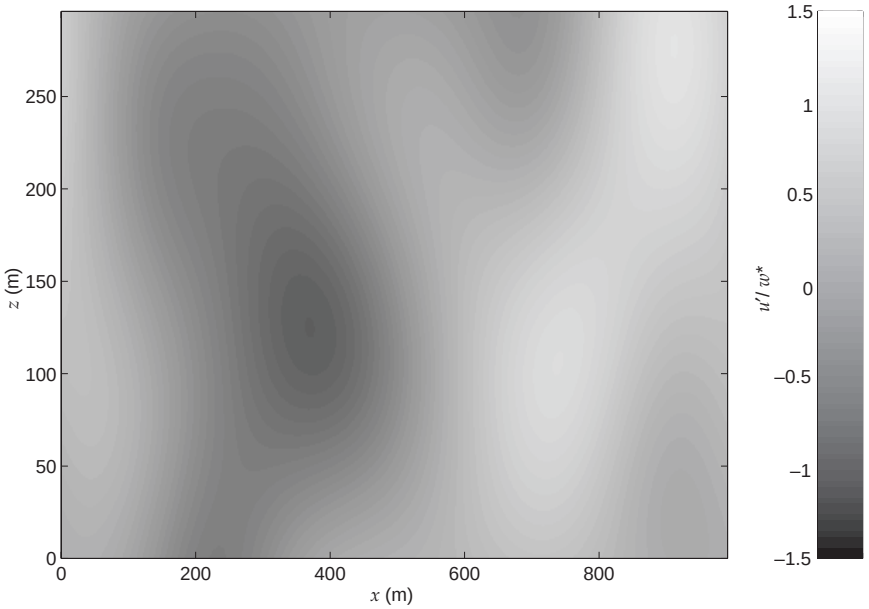

Figure 4. Synthesized turbulent velocity field for buoyantly driven turbulence, generated by a homogeneous von Kármán model.

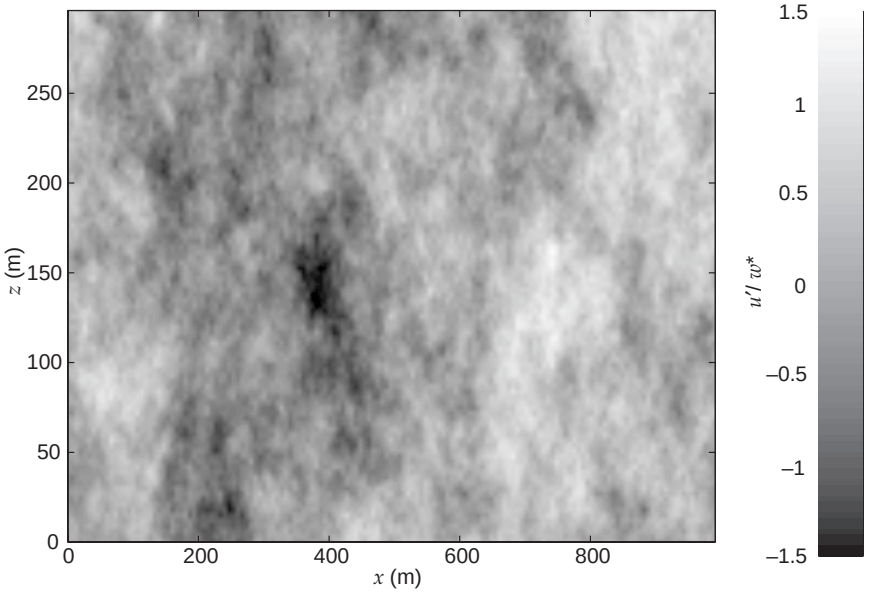

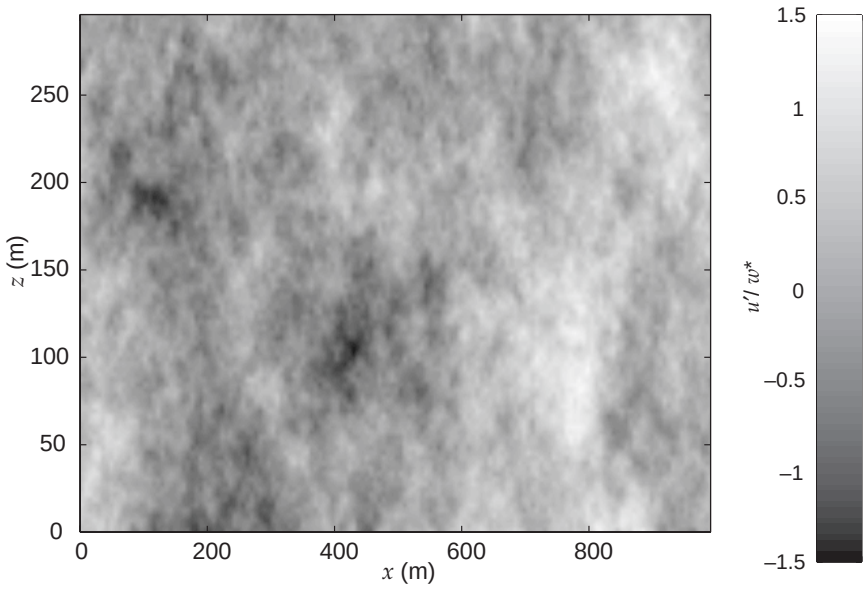

Figure 5. Synthesized turbulent velocity field for buoyantly driven turbulence, generated by Hunt/Graham/Wilson model.

The Gaussian model produces a much more smoothly varying field than the HGW and von Kármán models. Such smoothness is unrealistic for high-Reynolds-number turbulence such as the atmosphere. The HGW and von Kármán models are much more realistic, and yield quite similar results. There is a slight enhancement of the velocity fluctuations near the ground in the HGW model, which results from the ground blocking effect. (The differences between the HGW and von Kármán models are much more dramatic for the vertical velocity component. The horizontal velocity was plotted here, since it is more important for horizontal acoustic propagation.)

9.2 Small-Scale (Shear-Driven) Turbulence

The parameters values chosen for this set of examples are characteristic of turbulence generated by surface-layer wind shear. The integral length scale for this type of turbulence is proportional to the height. Five example synthesized turbulence fields are shown in figures 6 to 10. As before, the synthesized field is the in-plane horizontal velocity component. The resolution of the simulated fields is 200 grid points in the vertical direction and 300 in the horizontal.

The first of the synthesized fields (fig. 6) was created with an inhomogeneous Gaussian model with $\sigma^2 = 2.97u_*^2$, where u_* is called the *friction velocity*, and $L = 1.34z$, where z is the height. The second synthesized field (fig. 7) is an inhomogeneous von Kármán model, with $\sigma^2 = 2.97u_*^2$ and $\ell = 1.60z$. (The parameter values for both models are the ones derived for a shear-driven surface layer by Wilson, 1998.) The inhomogeneous Gaussian

Figure 6. Synthesized turbulent velocity field for shear-driven turbulence, generated by an inhomogeneous Gaussian model with height-dependent length scale.

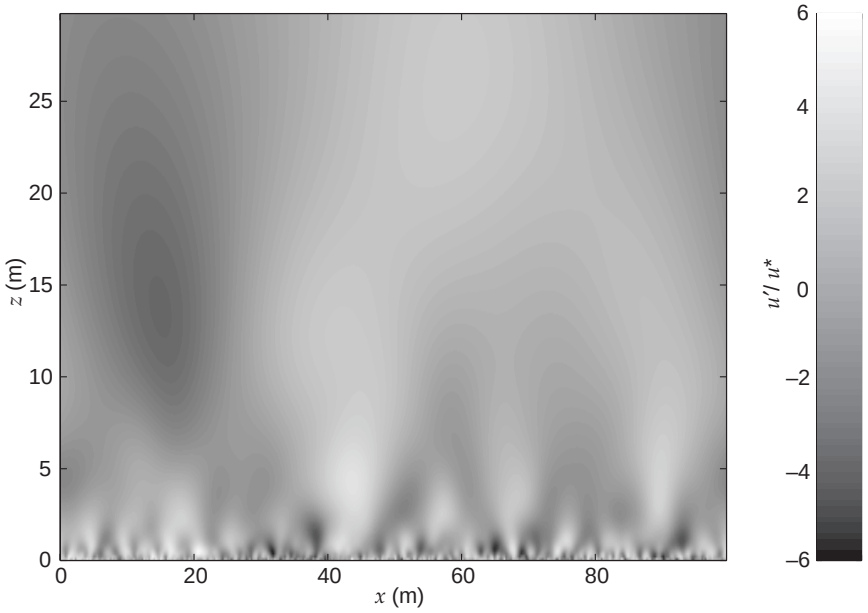

Figure 7. Synthesized turbulent velocity field for shear-driven turbulence, generated by an inhomogeneous von Kármán model with height-dependent length scale.

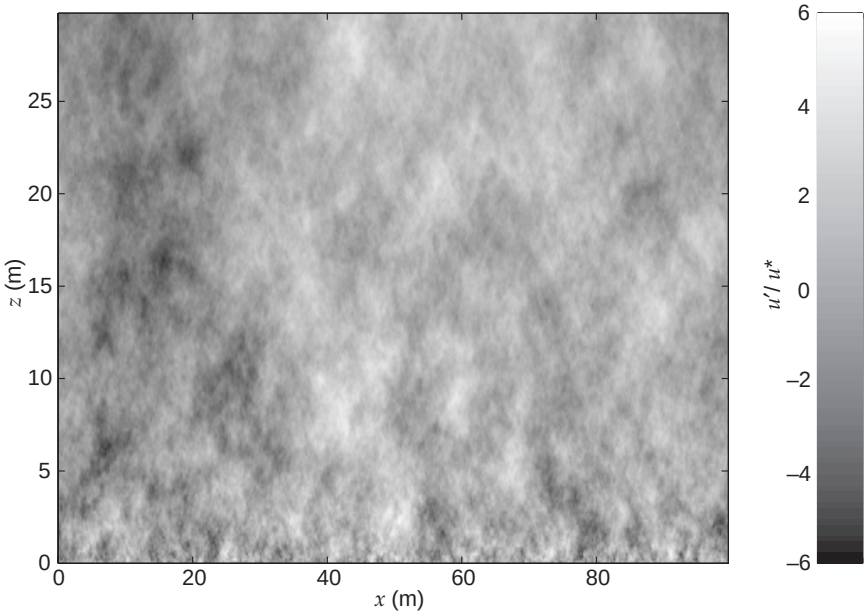

and von Kármán fields both clearly show small structures near the surface that gradually merge into larger ones away from the surface. However, the Gaussian model produces an unrealistically smooth field.

Figure 8 is a second example of a Gaussian field, differing from figure 6 in that the length scale has been assigned a constant (height-independent) value of $L = 1.1$ m. Although this value for L is rather unrealistic, it has often been used previously for acoustic wave scattering studies (Daigle et al., 1983, Daigle et al., 1986, Gilbert et al., 1990, Chevret et al., 1996). The resulting homogeneous field lacks the realistic merging of smaller structures into larger ones that was evident in figures 6 and 7.

The final two synthesized fields I consider, figures 9 and 10, were created with the Mann model. For reasons discussed in a previous report (Wilson, 1998), the parameter values used in the Mann model are $\Gamma = 3.53$, $\sigma^2 = 1.88u_*^2$, and $\ell = 0.805z$. Recall from section 8 that the spectra in the Mann model depend on the orientation relative to the wind. Figure 9 shows an along-wind vertical plane, while figure 10 is a crosswind vertical plane. Qualitatively, both fields are quite similar to the von Kármán model (fig. 7). Although it is difficult to discern visually, there is a statistical tendency for larger structures in the along-wind direction of the Mann model than in the von Kármán model. Some decrease of the variance in the crosswind direction is visually evident. It is interesting that the computations for the Mann model required about one day, which is significantly less than the HGW model, even though both models require numerical integrations. The Mann model ends up being faster because it is based mostly on simple algebraic functions, whereas the HGW model contains Bessel functions.

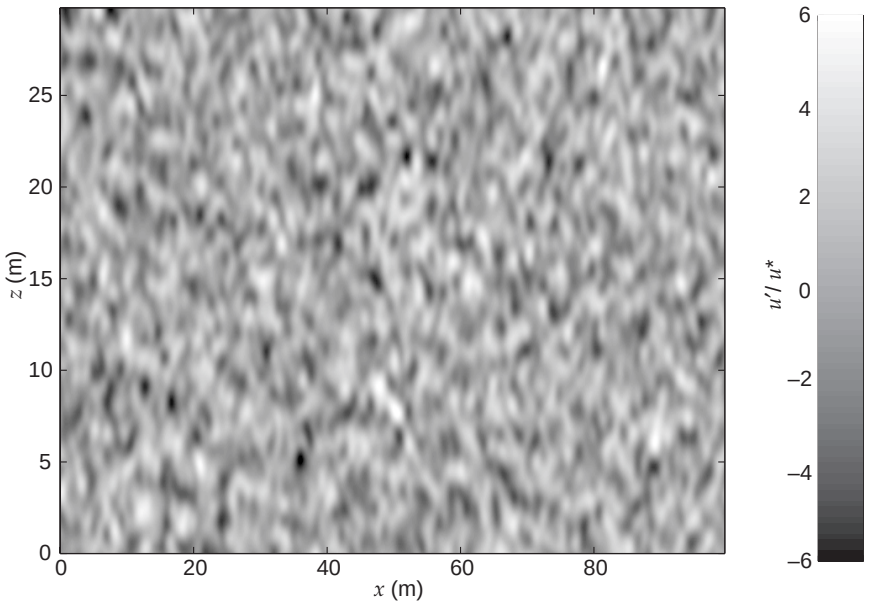

Figure 8. Synthesized turbulent velocity field for shear-driven turbulence, generated by a homogeneous Gaussian model with a constant (height-independent) length scale.

Figure 9. Synthesized turbulent velocity field for shear-driven turbulence, generated by Mann rapid-distortion model. Shown is a vertical plane parallel to wind; synthesized field is horizontal wind fluctuation parallel to mean wind.

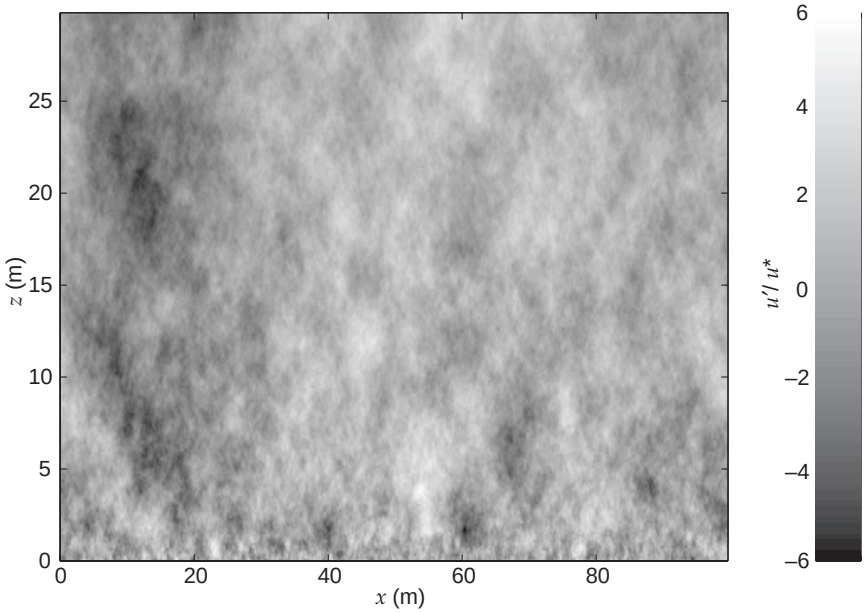

Figure 10. Synthesized turbulent velocity field for shear-driven turbulence, generated by Mann's rapid-distortion model. Shown is a vertical plane perpendicular to wind; synthesized field is horizontal wind fluctuation perpendicular to mean wind.

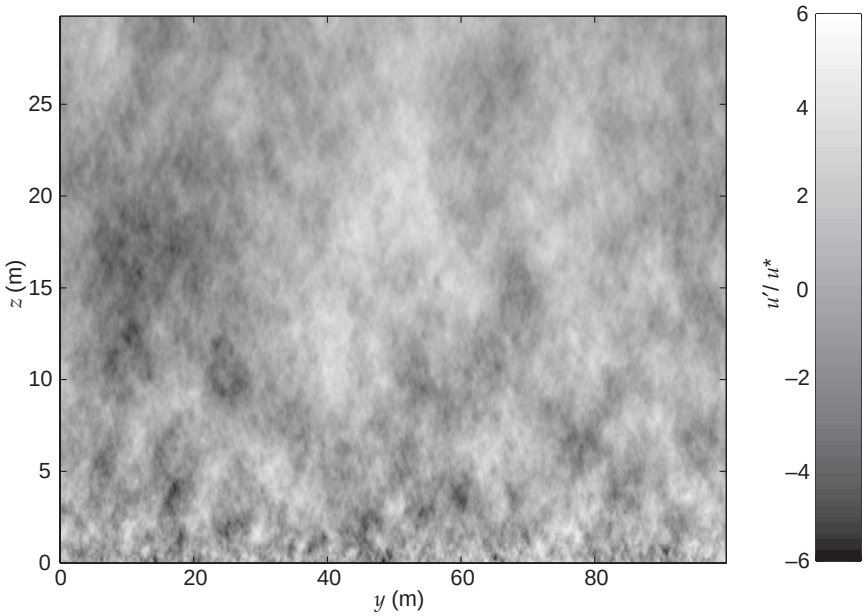

10. Concluding Remarks

A comprehensive set of equations for second-order statistical models of turbulence is derived in this report. Future research will involve application of these results to wave propagation calculations.

The generalized random-phase method (GRPM) described in this report for synthesizing inhomogeneous random fields provides much more realistic turbulence fields for use in wave propagation calculations than do previous methods. The method could also be applied to turbulent transport and diffusion calculations. When GRPM is used with the HGW and Mann turbulence models, the resulting synthesized fields have second-order statistics very close to the known properties of atmospheric turbulence.

Bibliography

Abramowitz, M., and I. A. Stegun (1965): *Handbook of Mathematical Functions*. Dover, San Francisco, pp 675–679.

Batchelor, G. K. (1953): *The Theory of Homogeneous Turbulence*. Cambridge Univ. Press, Cambridge, Great Britain.

Chevret, P., P. Blanc-Benon, and D. Juvé (1996): A numerical model for sound propagation through a turbulent atmosphere near the ground. *J. Acoust. Soc. Am.*, **100**, 3587–3599.

Daigle, G. A., T.F.W. Embleton, and J. E. Piercy (1986): Propagation of sound in the presence of gradients and turbulence near the ground. *J. Acoust. Soc. Am.*, **79**, 613–627.

Daigle, G. A., J. E. Piercy, and T.F.W. Embleton (1983): Line-of-sight propagation through atmospheric turbulence near the ground. *J. Acoust. Soc. Am.*, **74**, 1505–1513.

Deardorff, J. W. (1970a): Convective velocity and temperature scales for the unstable planetary boundary layer and for Rayleigh convection. *J. Atmos. Sci.*, **27**, 1211–1213.

Deardorff, J. W. (1970b): A numerical study of three-dimensional turbulent channel flow at large Reynolds numbers. *J. Fluid Mech.*, **41**, 453–480.

Gilbert, K. E., X. Di, and R. R. Korte (1996): Distorted-wave Born approximation analysis of sound levels in a refractive shadow zone. In *Seventh International Symposium on Long Range Sound Propagation*, Ecole Centrale de Lyon, Lyon, France, 373–389.

Gilbert, K. E., R. Raspet, and X. Di (1990): Calculation of turbulence effects in an upward refracting atmosphere. *J. Acoust. Soc. Am.*, **87**, 2428–2437.

Gradshteyn, I. S., and I. M. Ryzhik (1994): *Table of Integrals, Series, and Products*. Academic Press, San Diego.

Hunt, J.C.R. (1984): Turbulence structure in thermal convection and shear-free boundary layers. *J. Fluid Mech.*, **138**, 161–184.

Hunt, J.C.R., and J.M.R. Graham (1978): Free-stream turbulence near plane boundaries. *J. Fluid Mech.*, **84**, 209–235.

Juvé, D., P. Blanc-Benon, and P. Chevret (1994): Sound propagation through a turbulent atmosphere: Influence of the turbulence model. In *Proceedings of the Sixth International Symposium on Long Range Sound Propagation*, D. I. Havelock and M. R. Stinson, editors, NRC Canada, Ottawa, Canada, pp 270–282.

Kolmogorov, A. N. (1941): The local structure of turbulence in incompressible viscous fluid for very large Reynolds numbers. *C. R. Acad. Sci. URSS*, **30**, 301–305.

Lumley, J. L. (1971): *Stochastic Tools in Turbulence*. Academic Press, New York.

Mann, J. (1994): The spatial structure of neutral atmospheric surface layer turbulence. *J. Fluid Mech.*, **273**, 141–168.

Mellert, V., V. Ostashev, and R. Wandelt (1994): Sound scattering by scalar and vector random fields. In *Proceedings of the Sixth International Symposium on Long Range Sound Propagation*, D. I. Havelock and M. R. Stinson, editors, NRC Canada, Ottawa, Canada, pp 334–347.

Moeng, C.-H. (1984): A large-eddy-simulation model for the study of planetary boundary-layer turbulence. *J. Atmos. Sci.*, **41**, 2052–2062.

Moin, P., and R. D. Moser (1989): Characteristic-eddy decomposition of turbulence in a channel. *J. Fluid Mech.*, **200**, 471–509.

Ostashev, V. E. (1994): Sound propagation and scattering in media with random inhomogeneities of sound speed, density and medium velocity. *Waves Rand. Med.*, **4**, 403–428.

Tatarskii, V. I. (1971): *The Effects of the Turbulent Atmosphere on Wave Propagation*. Keter, Jerusalem.

Wilson, D. K. (1996): Empirical orthogonal function analysis of the weakly convective atmospheric boundary layer. Part I: Eddy structures. *J. Atmos. Sci.*, **53**, 801–823.

Wilson, D. K. (1997a): Performance of acoustic tracking arrays in atmospheric turbulence. U.S. Army Research Laboratory, ARL-TR-1286.

Wilson, D. K. (1997b): Three-dimensional correlation and spectral functions for turbulent velocities in homogeneous and surface-blocked boundary layers. U.S. Army Research Laboratory, ARL-TR-1287.

Wilson, D. K. (1997c): A three-dimensional correlation/spectral model for turbulent velocities in a convective boundary layer. *Bound. Layer Meteorol.*, **85**, 35–52.

Wilson, D. K. (1998): Anisotropic turbulence models for acoustic propagation through the neutral atmospheric surface layer. U.S. Army Research Laboratory, ARL-TR-1519.

Wilson, D. K., and D. W. Thomson (1994): Acoustic propagation through anisotropic, surface-layer turbulence. *J. Acoust. Soc. Am.*, **96**, 1080–1095.

Acronyms

1D (2D, 3D)	one- (two-, three-) dimensional
CBL	convective boundary layer
EOF	empirical orthogonal function
GRPM	generalized random-phase method
HGW	Hunt/Graham/Wilson model
RPM	random-phase method

Distribution

Admnstr
Defns Techl Info Ctr
Attn DTIC-OCP
8725 John J Kingman Rd Ste 0944
FT Belvoir VA 22060-6218

Mil Asst for Env Sci
Ofc of the Undersec of Defns for Rsrch & Engrg R&AT E LS
Pentagon Rm 3D129
Washington DC 20301-3080

Ofc of the Dir Rsrch and Engrg
Attn R Menz
Pentagon Rm 3E1089
Washington DC 20301-3080

Ofc of the Secy of Defns
Attn ODDRE (R&AT) G Singley
Attn ODDRE (R&AT) S Gontarek
The Pentagon
Washington DC 20301-3080

OSD
Attn OUSD(A&T)/ODDDR&E(R) R Trew
Washington DC 20301-7100

AMCOM MRDEC
Attn AMSMI-RD W C McCorkle
Redstone Arsenal AL 35898-5240

ARL Chemical Biology Nuc Effects Div
Attn AMSRL-SL-CO
Aberdeen Proving Ground MD 21005-5423

Army Communications Elec Ctr for EW RSTA
Attn AMSEL-EW-D
FT Monmouth NJ 07703-5303

Army Corps of Engrs Engr Topographics Lab
Attn ETL-GS-LB
FT Belvoir VA 22060

Army Dugway Proving Ground
Attn STEDP 3
Attn STEDP-MT-DA-L-3
Attn STEDP-MT-M Bowers
Dugway UT 84022-5000

Army Field Artillery School
Attn ATSF-TSM-TA
FT Sill OK 73503-5000

Army Foreign Sci Tech Ctr
Attn CM
220 7th Stret NE
Charlottesville VA 22901-5396

Army Infantry
Attn ATSH-CD-CS-OR E Dutoit
FT Benning GA 30905-5090

Army Materiel Sys Analysis Activity
Attn AMXSY-AT Campbell
Attn AMXSY-CS Bradley
Aberdeen Proving Ground MD 21005-5071

Army Missile Cmnd
Attn AMSMI-RD-AC-AD Peterson
Redstone Arsenal AL 35898-5242

Army Missile Cmnd
Attn AMSMI-RD-DE-SE G Lill Jr
Redstone Arsenal AL 35898-5245

Army Missile Cmnd
Attn AMSMI-RD-AS-SS R Alongi
Redstone Arsenal AL 35898-5253

Army Rsrch Ofc
Attn AMXRO-GS Bach
PO Box 12211
Research Triangle Park NC 27709

Army Strat Defns Cmnd
Attn CSSD-SL-L Lilly
PO Box 1500
Huntsville AL 35807-3801

Army TACOM-ARDEC
Attn AMSTA-AR-WEL-TL
Bldg 59 Phillips Rd
Picatinny Arsenal NJ 07806-5000

CECOM
Attn PM GPS COL S Young
FT Monmouth NJ 07703

CECOM
Sp & Terrestrial Commctn Div
Attn AMSEL-RD-ST-MC-M H Soicher
FT Monmouth NJ 07703-5203

Distribution (cont'd)

Dir for MANPRINT
Ofc of the Deputy Chief of Staff for Prsnnl
Attn J Hiller
The Pentagon Rm 2C733
Washington DC 20301-0300

Hdqtrs Dept of the Army
Attn DAMO-FDT D Schmidt
400 Army Pentagon Rm 3C514
Washington DC 20301-0460

Natl Security Agency
Attn W21 Longbothum
9800 Savage Rd
FT George G Meade MD 20755-6000

TACOM
Attn AMSTA-TR-R E Shalis
Mail Stop 263
Warren MI 48090

TECOM
Attn AMSTE-CL
Aberdeen Proving Ground MD 21005-5057

US Army ARDEC
Attn AMSTA-AR-FSF-RM J Heberley
Bldg 95N
Picatinny Arsenal NJ 07806

US Army Edgewood Rsrch, Dev, & Engrg Ctr
Attn SCBRD-TD J Vervier
Aberdeen Proving Ground MD 21010-5423

US Army Info Sys Engrg Cmnd
Attn ASQB-OTD F Jenia
FT Huachuca AZ 85613-5300

US Army Materiel Sys Analysis Activity
Attn AMXSY-CR Marchetti
Attn AMXSY-D J McCarthy
Aberdeen Proving Ground MD 21005-5071

US Army Mis Cmnd (USAMICOM)
Attn AMSMI-RD-CS-R Documents
Redstone Arsenal AL 35898-5400

US Army Natick Rsrch, Dev, & Engrg CtrActing Techl Dir
Attn SSCNC-T P Brandler
Natick MA 01760-5002

US Army Nuclear & Chem Agency
Attn MONA-ZB
Bldg 2073
Springfield VA 22150-3198

US Army OEC
Attn CSTE-EFS
Park Center IV 4501 Ford Ave
Alexandria VA 22302-1458

US Army Rsrch Ofc
Attn G Iafrate
4300 S Miami Blvd
Research Triangle Park NC 27709

US Army Simulation, Train, & Instrmntn Cmnd
Attn J Stahl
12350 Research Parkway
Orlando FL 32826-3726

US Army Tank-Automtv & Armaments Cmnd
Attn AMSTA-AR-TD C Spinelli
Bldg 1
Picatinny Arsenal NJ 07806-5000

US Army Tank-Automtv Cmnd Rsrch, Dev, & Engrg Ctr
Attn AMSTA-TA J Chapin
Warren MI 48397-5000

US Army Test & Eval Cmnd
Attn R G Pollard III
Aberdeen Proving Ground MD 21005-5055

US Army TRADOC Anlys Cmnd—WSMR
Attn ATRC-WSS-R
White Sands Missile Range NM 88002

US Army Train & Doctrine Cmnd Battle Lab Integration & Techl Dirctrt
Attn ATCD-B J A Klevecz
FT Monroe VA 23651-5850

US Military Academy
Dept of Mathematical Sci
Attn MAJ D Engen
West Point NY 10996

USACRREL
Attn CEREL-GP R Detsch
72 Lyme Rd
Hanover NH 03755-1290

Distribution (cont'd)

USATRADOC
Attn ATCD-FA
FT Monroe VA 23651-5170

Nav Air War Cen Wpn Div
Attn CMD 420000D C0245 A Shlanta
1 Admin Cir
China Lake CA 93555-6001

Nav Surface Warfare Ctr
Attn Code B07 J Pennella
17320 Dahlgren Rd Bldg 1470 Rm 1101
Dahlgren VA 22448-5100

Naval Surface Weapons Ctr
Attn Code G63
Dahlgren VA 22448-5000

Air Weather Service
Attn TechL Lib FL4414 3
Scott AFB IL 62225-5458

GPS Joint Prog Ofc Dir
Attn COL J Clay
2435 Vela Way Ste 1613
Los Angeles AFB CA 90245-5500

Hdqtrs AFWA/DNX
106 Peacekeeper Dr Ste 2N3
Offutt AFB NE 68113-4039

Phillips Laboratory
Attn PL/LYP Chisholm
Hanscom AFB MA 01731-5000

USAF Rome Lab Tech
Attn Corridor W Ste 262 RL SUL
26 Electr Pkwy Bldg 106
Griffiss AFB NY 13441-4514

USAFETAC DNE
Attn Glauber
Scott AFB IL 62225-5008

DARPA
Attn B Kaspar
Attn L Stotts
3701 N Fairfax Dr
Arlington VA 22203-1714

NASA Marshal Space Flt Ctr Atmospheric Sciences Div
Attn E501 Fichtl
Huntsville AL 35802

NASA Spct Flt Ctr Atmospheric Sciences Div
Attn Code ED 41 1
Huntsville AL 35812

ARL Electromag Group
Attn Campus Mail Code F0250 A Tucker
University of Texas
Austin TX 78712

Univ of Mississippi NCPA
Attn H E Bass
University MS 38577

Dept of Commerce Ctr
Mountain Administration
Attn Spprt Ctr Library R51
325 S Broadway
Boulder CO 80303

Natl Ctr for Atmospheric Research
Attn NCAR Library Serials
PO Box 3000
Boulder CO 80307-3000

NCSU
Attn J Davis
PO Box 8208
Raleigh NC 27650-8208

US Army Rsrch Lab
Attn AMSRL-CI-LL Techl Lib (3 copies)
Attn AMSRL-CS-AL-TA Mail & Records Mgmt
Attn AMSRL-CS-EA-TP Techl Pub (3 copies)
Attn AMSRL-IS-E Battlefield Environ Div
Attn AMSRL-IS-EE C Williamson
Attn AMSRL-IS-EE D K Wilson
Attn AMSRL-IS-EE J Martin
Attn AMSRL-IS-EE R Loucks
Attn AMSRL-SE-EE Z G Sztankay
Attn AMSRL-SE-SA N Srour
Adelphi MD 20783-1197

REPORT DOCUMENTATION PAGE

Form Approved
OMB No. 0704-0188

1. AGENCY USE ONLY *(Leave blank)*	2. REPORT DATE	3. REPORT TYPE AND DATES COVERED
	July 1998	Final, October 1996 to February 1998

4. TITLE AND SUBTITLE
Turbulence Models and the Synthesis of Random Fields for Acoustic Wave Propagation Calculations

5. FUNDING NUMBERS
DA PR: B53A
PE: 61102A

6. AUTHOR(S)
D. Keith Wilson

7. PERFORMING ORGANIZATION NAME(S) AND ADDRESS(ES)
U.S. Army Research Laboratory
Attn: AMSRL-IS-EE (dkwilson@arl.mil)
2800 Powder Mill Road
Adelphi, MD 20783-1197

8. PERFORMING ORGANIZATION REPORT NUMBER
ARL-TR-1677

9. SPONSORING/MONITORING AGENCY NAME(S) AND ADDRESS(ES)
U.S. Army Research Laboratory
2800 Powder Mill Road
Adelphi, MD 20783-1197

10. SPONSORING/MONITORING AGENCY REPORT NUMBER

11. SUPPLEMENTARY NOTES
AMS code: 61110253A11
ARL PR: 8FEJ60

12a. DISTRIBUTION/AVAILABILITY STATEMENT
Approved for public release; distribution unlimited.

12b. DISTRIBUTION CODE

13. ABSTRACT *(Maximum 200 words)*

A comprehensive set of equations is derived for correlations and spectra of atmospheric turbulence, useful for wave propagation calculations and other applications. Three basic turbulence models are considered: the Gaussian, von Kármán, and Kolmogorov models. Two extended forms of the von Kármán model are also described: the Mann model for a shear-driven atmospheric surface layer, and the Hunt/Graham/Wilson model for a convective boundary layer. A new method for synthesizing random fields from an inhomogeneous spectral model, called the generalized random-phase method, is described and applied to the various turbulence models.

14. SUBJECT TERMS
Turbulence models, empirical orthogonal functions, wave propagation, random field synthesis

15. NUMBER OF PAGES
62

16. PRICE CODE

17. SECURITY CLASSIFICATION OF REPORT	18. SECURITY CLASSIFICATION OF THIS PAGE	19. SECURITY CLASSIFICATION OF ABSTRACT	20. LIMITATION OF ABSTRACT
Unclassified	Unclassified	Unclassified	UL

NSN 7540-01-280-5500

Standard Form 298 (Rev. 2-89)
Prescribed by ANSI Std. Z39-18
298-102